Journal of Non-Newtonian Fluid Mechanics 283 (2020) 104335

Contents lists available at ScienceDirect

Journal of Non-Newtonian Fluid Mechanics

journal homepage: www.elsevier.com/locate/jnnfm

A domain decomposition approach to accelerate simulations of structure preserving nematic liquid crystal models

Sylver Carter[a,1], Amit Rotem[b,2], Shawn W. Walker[c,3,*]

[a] Department of Mathematics, University of North Alabama, 1 Harrison Plaza, Florence, AL 35632, USA
[b] Department of Applied Mathematics and Statistics, Colorado School of Mines, 1500 Illinois St., Golden, CO 80401, USA
[c] Department of Mathematics and Center for Computation and Technology (CCT), Louisiana State University, Baton Rouge, LA 70803, USA

ARTICLE INFO

MSC:
65N30
49M25
35J70

Keywords:
Liquid crystals
Defects
Degenerate elliptic
Finite element method
Alternating Schwarz method

ABSTRACT

We present a method for speeding up equilibrium simulations of liquid crystals for two related models that are degenerate with respect to defects: the Ericksen model and the uniaxially constrained Landau-de Gennes model. The degeneracy induces a non-linear/non-smooth coupling between the two order parameters in both models that makes the discrete problems very stiff to solve. The technique described in this paper uses an alternating Schwarz domain decomposition method that isolates the degenerate region and alleviates some of the stiffness, and is easy to implement. We present numerical results illustrating the speed-up and how it is affected by the size of the sub-domains and the number of sub-iterations used within the degenerate region.

1. Introduction

Liquid crystals (LCs) continue to be developed into new technologies that take advantage of their optical, electric/magnetic, and mechanical properties [1,2]. The most well-known aspect of LCs are their optical properties [3–7] which have found newer uses in electronic shutters [8] and novel types of lasers [9,10]. Moreover, LCs affinity for electric and magnetic fields is well-established [11–13] which is used to enable new types of devices [14,15]. Furthermore, LCs are an integral component of elastomeric materials [16–19], which can enable dynamic shape control of elastic bodies [20,21]. Indeed, a key requirement for creating complex structured materials [22,23] is to take advantage of novel forms of self-assembly [24–26]. In particular, LCs coupled with colloidal particle effects [27–30] can enable functionalized materials [31–33].

Naturally, numerical computation is a critical tool to enable the exploration of LC physics and device design [34–36]. An extensive body of research exists on simulation methods for a variety of LC modeling situations [37]. Some approaches focus on equilibrium states of LCs possibly coupled with external effects [38–45], while others tackle dynamic LC systems [46–50]. See [51–60] for more references on the numerical analysis of LCs.

In this paper, we describe a method for speeding up equilibrium simulations of LCs for two different, but related, models of LCs: the Ericksen model [57,58,61], and the uniaxially constrained Landau-deGennes model [62–64]. The hallmark of these models is that the Euler-Lagrange equation is a degenerate elliptic partial differential equation (PDE) [52,55,65,66]. The nature of the degeneracy induces a non-linear coupling between the two order parameters of the system that leads to a kind of non-standard "stiffness" when solving a linearized gradient flow to find local minimizers. We describe an alternating Schwarz method that can alleviate some of this stiffness. Indeed, it is able to reduce the simulation time (for finding a local minimizer) while preserving our robust gradient flow methods (monotone energy decreasing) [41,42,55–57], and is still easy to implement.

Remark 1 (Main Contribution)**.** Computing minimizers of LC models, when defects are present, is difficult. Indeed, applying straightforward numerical procedures to these models suffer from slow convergence to the minimizer because of the singular nature of defects. This paper shows that isolating the defect region with a domain decomposition approach can help speed up gradient flow schemes and converge to the minimizer faster.

* Corresponding author.
E-mail addresses: arotem@mymail.mines.edu (A. Rotem), walker@math.lsu.edu (S.W. Walker).

[1] S. Carter acknowledges financial support by the NSF OAC-1852454 (REU), and support by HPC@LSU computing.
[2] A. Rotem acknowledges financial support by the NSF OAC-1852454 (REU), and support by HPC@LSU computing.
[3] S. W. Walker acknowledges financial support by the NSF DMS-1555222 (CAREER), and support by HPC@LSU computing.

https://doi.org/10.1016/j.jnnfm.2020.104335
Received 7 April 2020; Received in revised form 19 June 2020; Accepted 20 June 2020
Available online 25 June 2020

An outline is as follows. Section 2 reviews the Ericksen model and the Landau-de Gennes (LdG) model of LCs; for the LdG model, the focus is on including the uniaxial constraint which yields a model similar to the Ericksen model with respect to the singularity of defects. Section 3 reviews the finite element discretization of the Ericksen model only (we defer to [63,64] for the uniaxial LdG discretization). In Section 4, we describe the gradient flow scheme for the discrete Ericksen energy (the scheme for the uniaxial LdG method is similar and can be found in [63,64]). In addition, we explain the domain decomposition approach that we use to augment the gradient flow. Section 5 presents numerical results showing how convergence is affected by the domain decomposition approach. Section 6 gives some concluding remarks.

2. Liquid crystal models

A standard model for LCs is the Landau-deGennes model that uses a mesoscopic order parameter $\mathbf{Q}$, which is a $d \times d$ matrix in $\mathbb{R}^d$, that is motivated by an ensemble type of averaging [67,68]. With the tools of classical continuum mechanics, one can formulate an energy functional which the LC material minimizes at equilibrium (i.e. the Landau-deGennes energy). Mathematical analysis of the $\mathbf{Q}$-tensor model has been done in several works; for instance, see [38,69–74].

On the other hand, the Oseen-Frank model is the simplest, macroscopic model of a nematic LC [68,75,76], which uses a *unit* vector field $\mathbf{n}(\mathbf{x}) \in \mathbb{R}^d$ (the *director*) as the order parameter. The energy functional (in the one-constant case) is given by $\int_\Omega |\nabla \mathbf{n}|^2$. Despite being a workhorse of the display industry [4,77,78], it suffers a major drawback in that defects (discontinuities in $\mathbf{n}$), such as point defects in $\mathbb{R}^2$ and line defects in $\mathbb{R}^3$ have infinite energy.

In this paper, we focus on two different LC models. The first is the one-constant Ericksen model (Section 2.1), and the second is a uniaxially constrained version of the Landau-deGennes $\mathbf{Q}$-model (Section 2.2). The hallmark of these models is an elliptic degeneracy that is directly connected to fundamental symmetries in the LC material, which induces a non-trivial kind of "stiffness" in the equations to solve to find a minimizer. The main contribution of this paper is an alternating Schwarz method that is able to alleviate this stiffness which we justify with extensive computational evidence.

Throughout the paper, we assume Ω is a bounded Lipschitz domain in $\mathbb{R}^d$ with $d = 2$, or 3, representing the LC domain. We use standard notation for $L^2(\mathcal{D})$, $[L^2(\mathcal{D})]^d$, $[L^2(\mathcal{D})]^{d\times d}$ inner products throughout: $(u, v)_\mathcal{D} := \int_\mathcal{D} uv$, $(\mathbf{u}, \mathbf{v})_\mathcal{D} := \int_\mathcal{D} \mathbf{u} \cdot \mathbf{v}$, $(\mathbf{M}, \mathbf{Y})_\mathcal{D} := \int_\mathcal{D} \mathbf{M} : \mathbf{Y}$, where $\mathcal{D}$ is a generic domain. We simplify the notation with $(u, v) \coloneqq (u, v)_\Omega$ when integrating over Ω. Integrals over co-dimension 1 subsets, such as $\Gamma \subset \partial\Omega$, always use a subscript, e.g. $(u, v)_\Gamma$.

2.1. Ericksen's model

The Ericksen model uses two order parameters: a *director* field $\mathbf{n} : \Omega \to \mathbb{S}^{d-1}$, i.e. a vector-valued function with unit length point-wise, and a *degree-of-orientation* scalar field $s : \Omega \subset \mathbb{R}^d \to [-1/(d-1), 1]$. The director represents an average alignment of LC molecules at a macroscopic level. Since $|\mathbf{n}| = 1$, it cannot describe a "loss of order" in the liquid crystal material. The s variable models how well aligned the individual LC molecules are with $\mathbf{n}$ and s may vanish which means the LC molecules have no net alignment in any direction. See [57,68] for more details on the meaning of $\mathbf{n}$ and s.

Remark 2. The use of a vector field for $\mathbf{n}$ has an important limitation. Nematic LCs are usually treated as having a reflection symmetry along their main axis, which means they are best represented by a *line segment*, not a vector that has a *direction*. This means that the Ericksen model cannot capture half-integer defects, which do occur in some LC experiments (depending on boundary conditions) [71,72].

Despite this, Ericksen provides a simple model to demonstrate the domain decomposition approach in this paper. In particular, integer defects are modeled correctly by Ericksen and defects play a critical role in the speed of convergence of the algorithm. In Section 2.2, we introduce the $\mathbf{Q}$-model, which does not have this orientation limitation.

2.1.1. Ericksen's simple energy

Ericksen's model seeks a minimizer $(s, \mathbf{n})$ of a free energy functional, whose simplest form is the following (dimensional) energy:

$$E_{\text{erk}}[s, \mathbf{n}] = E_{\text{s}}[s, \mathbf{n}] + \int_\Omega \psi(s) dx,$$
$$E_{\text{s}}[s, \mathbf{n}] := \frac{1}{2} \int_\Omega \left(b_0 |\nabla s|^2 + k_0 s^2 |\nabla \mathbf{n}|^2 \right) dx, \tag{1}$$

where b_0, $k_0 > 0$ are model parameters with typical physical values for $k_0 \approx 10^{-11}$ J/m [79, Table 1, pg. 168]. We are unaware of experimental data for b_0, so we assume $b_0 = O(k_0)$.

The double well potential ψ is a C^2 function defined on $-1/(d-1) < s < 1$ that satisfies [61,65,66]

(i) $\lim_{s\to 1} \psi(s) = \lim_{s\to -1/(d-1)} \psi(s) = \infty$,
(ii) $\psi(0) > \psi(s^*) = \min_{s\in[-1/(d-1),1]} \psi(s) = 0$ for some $s^* \in (0, 1)$,
(iii) $\psi'(0) = 0$.

Remark 3. The form of ψ follows from the (uniaxial) Landau-deGennes theory of nematic LCs [1,68]. Often, the following choice is made:

$$\psi(s) = \frac{A'}{2} s^2 - \frac{B'}{3} s^3 + \frac{C'}{4} s^4, \tag{2}$$

which is connected to the Landau-deGennes theory (see Section 2.2.2). The parameters A', B', C' depend on the material with B', C' positive and A' having no definite sign. Usually, A' is proportional to a temperature difference [80] having the form $A' \propto (T - T^*)$, where T is the actual temperature and T^* is the super-cooling temperature. Physical values for A', B', and C' are approximately 10^5 J/m^3 [79, Table 1, pg. 168].

Choosing (2) for ψ automatically satisfies property (iii). If A' is bounded by a sufficiently small positive number A'_0, then property (ii) is also satisfied (this corresponds to having a stable nematic phase). Alternatively, if A' is very large (positive), then the only stable phase is the isotropic phase, meaning $s = 0$ everywhere. Property (i) is not satisfied by (2). However, the s^4 term can be modified near the bounds $s = -1/(d-1), +1$ to enforce property (i), without affecting the stability of the nematic phases.

To make the numerics simpler, we assume the form of (2) for ψ, however, one can add barrier/penalty functions to enforce property (i).

When the degree of orientation s is a non-zero constant, the energy $E_{\text{s}}[s, \mathbf{n}]$ is essentially the Oseen-Frank free energy $\int_\Omega |\nabla \mathbf{n}|^2$. With discontinuities in $\mathbf{n}$ (i.e. defects), the degree of orientation s will vanish in the vicinity of the defect to avoid a singular energy. Thus, defects in $\mathbf{n}$ must occur in the singular set

$$\{x \in \Omega : \ s(x) = 0\}. \tag{3}$$

Existence of minimizers was shown in [65,66] and analytic solutions for minimizers with defects were constructed in [68]. Minimizers with other types of defect structures were discovered numerically in [55].

Remark 4. An obvious approach to the Ericksen energy is to regularize it, e.g. replace $E_{\text{s}}[s, \mathbf{n}]$ by $E^\epsilon_{\text{s}}[s, \mathbf{n}] = \frac{1}{2} \int_\Omega (b_0 |\nabla s|^2 + k_0 (s^2 + \epsilon^2) |\nabla \mathbf{n}|^2)$ for some finite $\epsilon > 0$ as was done in [52,81]. Unfortunately, this fundamentally changes the Ericksen model into a variant of Oseen-Frank, implying that point defects in two dimensions, and line defects in three dimensions, will give $E^\epsilon_{\text{s}}[s, \mathbf{n}] = +\infty$. Therefore, when defects are important, and they often are, a simple regularization approach *does not work*.

2.1.2. Non-dimensionalization

We now non-dimensionalize the energy in (1) (see also [80]); note that s and $\mathbf{n}$ are already non-dimensional. Let A'_0 be the characteristic scale for the double well (see Remark 3), and define $\epsilon_{\text{dw}} := \sqrt{k_0/(A'_0 R_0^2)}$, where $R_0 = \text{diam}(\Omega)$ is the length scale. Then, (1) becomes

$$E_{\text{erk}}[s,\mathbf{n}] \;=\; k_0 R_0 \overline{E}_{\text{erk}}[s,\mathbf{n}], \quad \overline{E}_{\text{erk}}[s,\mathbf{n}] = \overline{E}_{\text{s}}[s,\mathbf{n}] + \frac{1}{\epsilon_{\text{dw}}^2}\overline{E}_{\text{dw}}[s],$$
$$\overline{E}_{\text{dw}}[s] \;:=\; \int_{\overline{\Omega}} \bar{\psi}(s)\, d\mathbf{x} = (\bar{\psi}(s), 1), \quad \bar{\psi}(s) = \frac{1}{A_0'}\psi(s), \tag{4}$$

$$\overline{E}_{\text{s}}[s,\mathbf{n}] := \frac{1}{2}\int_{\overline{\Omega}} \left(\bar{b}_0|\nabla s|^2 + s^2|\nabla \mathbf{n}|^2\right) d\mathbf{x} = \frac{1}{2}\left[\bar{b}_0(\nabla s, \nabla s) + (s\nabla\mathbf{n}, s\nabla\mathbf{n})\right], \tag{5}$$

where $\bar{b}_0 = b_0/k_0$, $\bar{\psi}(s)$, $\overline{E}_{\text{s}}[s,\mathbf{n}]$, and $\overline{E}_{\text{dw}}[s]$ are non-dimensional, as well as the domains. For the rest of the paper, we deal with $\overline{E}_{\text{erk}}[s,\mathbf{n}]$ and drop the "bar" from the non-dimensional quantities for simplicity (i.e. we ignore the pre-factor k_0R_0 in $E_{\text{erk}}[s,\mathbf{n}]$).

2.1.3. Function space framework

An auxiliary variable $\mathbf{u} := s\mathbf{n}$ and identity was introduced in [65,66] that allows the energy $E_{\text{s}}[s,\mathbf{n}]$ to be rewritten as

$$E_{\text{s}}[s,\mathbf{n}] = \widetilde{E}_{\text{s}}[s,\mathbf{u}] := \frac{1}{2}\int_{\Omega} \left((b_0-1)|\nabla s|^2 + |\nabla \mathbf{u}|^2\right) dx, \tag{6}$$

which follows from $\nabla\mathbf{u} = \mathbf{n}\otimes\nabla s + s\nabla\mathbf{n}$ and the unit length constraint $|\mathbf{n}| = 1$. This suggests the following choice for the (closed) admissible set of minimizers [65,66]:

$$\mathcal{A} := \{(s,\mathbf{n}) \in H^1(\Omega) \times [L^\infty(\Omega)]^d \;:\; (s,\mathbf{u},\mathbf{n}) \text{ satisfies (8), with } \mathbf{u}\in[H^1(\Omega)]^d\}, \tag{7}$$

where

$$\mathbf{u} = s\mathbf{n}, \quad -1/(d-1) \le s \le 1 \text{ a.e. in } \Omega, \text{ and}$$
$$\mathbf{n} \in \mathbb{S}^{d-1} \text{ a.e. in } \Omega, \tag{8}$$

is called the *structural condition* of $\mathcal{A}$. If we write $(s,\mathbf{u},\mathbf{n})$ in $\mathcal{A}$, we mean that $(s,\mathbf{n})$ in $\mathcal{A}$, $\mathbf{u}$ in $[H^1(\Omega)]^d$, and $(s,\mathbf{u},\mathbf{n})$ satisfies (8). Note: the identity (6) only holds for $(s,\mathbf{u},\mathbf{n})$ in $\mathcal{A}$.

Remark 5. The purpose of the variable $\mathbf{u} = s\mathbf{n}$ is to make sense of the functional analytic framework in which the Ericksen model, at the continuous level, makes sense. The numerical algorithm does not use $\mathbf{u}$ in any way, but $\mathbf{u}$ is needed to justify the convergence of the method.

2.1.4. Boundary conditions

Boundary conditions are captured by functions $g : \mathbb{R}^d \to \mathbb{R}$, $\mathbf{r},\mathbf{q} : \mathbb{R}^d \to \mathbb{R}^d$ that satisfy the following.

Assumption 6 (Boundary Data is Regular)**.** There exists $g \in W^{1,\infty}(\mathbb{R}^d)$, $\mathbf{r} \in [W^{1,\infty}(\mathbb{R}^d)]^d$, $\mathbf{q} \in [L^\infty(\mathbb{R}^d)]^d$, such that $(g,\mathbf{r},\mathbf{q})$ satisfies (8) on $\mathbb{R}^d$, i.e. $\mathbf{r} = g\mathbf{q}$ and $\mathbf{q} \in \mathbb{S}^{d-1}$ a.e. in $\mathbb{R}^d$. Furthermore, we assume there is a fixed $\rho_0 > 0$ such that

$$\rho_0 \le g \le 1 - \rho_0. \tag{9}$$

Note that $\mathbf{q} \in [W^{1,\infty}(\{|g| > \epsilon\})]^d$, for all $\epsilon > 0$.

Weak anchoring conditions [57,58,68] are sometimes used in LC models as a way to enforce boundary conditions through energetic penalty terms. For simplicity, we use strong (Dirichlet) boundary conditions for both s and $\mathbf{n}$ on the whole boundary $\Gamma := \partial\Omega$. Thus, the admissible class, with boundary conditions, is given by

$$\mathcal{A}(g,\mathbf{q}) := \left\{(s,\mathbf{n}) \in \mathcal{A} \;:\; s|_\Gamma = g, \quad \mathbf{n}|_\Gamma = \mathbf{q}\right\}, \tag{10}$$

where we use a similar abuse of notation as above when writing $(s,\mathbf{u},\mathbf{n})$ in $\mathcal{A}(g,\mathbf{q})$. Note: $\mathbf{n}$ is H^1 in a neighborhood of Γ. Therefore, the minimization problem is as follows [65,66]

$$\min_{(s,\mathbf{n})\in\mathcal{A}(g,\mathbf{q})} E_{\text{erk}}[s,\mathbf{n}]. \tag{11}$$

This paper is concerned with a domain decomposition approach for speeding up the computation of minimizers with defects for the Ericksen and uniaxially constrained Landau-deGennes model. Hence, we refer to [55,57,58] for more details on the theory behind the Ericksen model.

2.2. The Landau-deGennes model

We follow [1,38,39,82] for the standard Landau-deGennes (LdG) model.

2.2.1. The Q model

We first present the LdG model in $\mathbb{R}^3$ ($d = 3$). LdG uses a tensor-valued order parameter $\mathbf{Q} : \Omega \to \mathbb{R}^{3\times3}$, which satisfies

$$\mathbf{Q} \in \mathbf{\Lambda} := \left\{\mathbf{Q} \in \mathbb{R}^{3\times3} \mid \mathbf{Q} = \mathbf{Q}^T,\ \text{tr}\ \mathbf{Q} = 0\right\}. \tag{12}$$

i.e. is symmetric and traceless. To understand the meaning of $\mathbf{Q}$, let us express $\mathbf{Q}$ (at some point in Ω) in its eigenframe:

$$\mathbf{Q} = s_1(\mathbf{n}_1\otimes\mathbf{n}_1) + s_2(\mathbf{n}_2\otimes\mathbf{n}_2) - \tfrac{1}{3}(s_1+s_2)\mathbf{I}, \tag{13}$$

where $\mathbf{n}_1, \mathbf{n}_2$ are orthonormal eigenvectors of $\mathbf{Q}$, with eigenvalues given by $\lambda_1 = \frac{2s_1-s_2}{3}$, $\lambda_2 = \frac{2s_2-s_1}{3}$, $\lambda_3 = -\frac{s_1+s_2}{3}$, where λ_3 corresponds to the eigenvector $\mathbf{n}_3 \perp \mathbf{n}_1, \mathbf{n}_2$. For physical reasons, the eigenvalues should lie in the interval $[-1/3, 2/3]$.

If all eigenvalues are equal, since $\mathbf{Q}$ is traceless, $\lambda_1 = \lambda_2 = \lambda_3 = 0$ and $s_1 = s_2 = 0$, i.e. $\mathbf{Q} = \mathbf{0}$ and the distribution of LC molecules is isotropic [68]. If two eigenvalues are equal, i.e.

$$\begin{aligned} \lambda_1 = \lambda_2 \quad &\Leftrightarrow \quad s_1 = s_2, \\ \lambda_1 = \lambda_3 \quad &\Leftrightarrow \quad s_1 = 0, \\ \lambda_2 = \lambda_3 \quad &\Leftrightarrow \quad s_2 = 0, \end{aligned} \tag{14}$$

then we call this state *uniaxial*, because it has one main eigenvector (the other two are indistinguishable). In this case, $\mathbf{Q}$ has the form

$$\mathbf{Q} = s\left(\mathbf{n}\otimes\mathbf{n} - \tfrac{1}{3}\mathbf{I}\right), \tag{15}$$

where $\mathbf{n}$ is the main eigenvector with eigenvalue $\lambda = (2/3)s$; the other two eigenvalues equal $-(1/3)s$. Because of the range of the eigenvalues, $s \in [-1/2, 1]$. If all three eigenvalues are distinct, then the state is called *biaxial*, and $\mathbf{Q}$ has the general form (13).

Let us focus on the uniaxial case. The variable s has the same meaning here as in Ericksen's model. But now $\mathbf{n}$ has been replaced by $\mathbf{n}\otimes\mathbf{n}$, which does not suffer from the orientation issue (see Remark 2). Indeed, $\mathbf{n}\otimes\mathbf{n}$ can represent the average orientation of the LC molecules in the sense of line segments (i.e. no artificial orientation). In the biaxial case, four parameters (s_1, s_2, $\mathbf{n}_1\otimes\mathbf{n}_1$, $\mathbf{n}_2\otimes\mathbf{n}_2$) are necessary to capture the two "modes" of alignment that LC molecules could have.

Remark 7. For the LdG model, the standard analytic treatment is to deal with $\mathbf{Q}$ directly, i.e. we do not separate it into the constituent parts: s_1, s_2, $\mathbf{n}_1\otimes\mathbf{n}_1$, $\mathbf{n}_2\otimes\mathbf{n}_2$. Instead, we have

$$\mathbf{Q} \in \mathbf{\Lambda} \quad \Leftrightarrow \quad \mathbf{Q} = \begin{bmatrix} q_{11} & q_{12} & q_{13} \\ & q_{22} & q_{23} \\ & & q_{33} \end{bmatrix}, \text{ where } q_{33} := -q_{11} - q_{22}, \tag{16}$$

where the lower triangular terms are, of course, determined by symmetry. This makes the analytical framework more direct, and the numerical method more straightforward than in the Ericksen model. However, a drawback is that the computational effort may be higher because there are five independent variables to compute. In addition, the structure of uniaxial minimizers may not be respected [63,64] (see Section 2.3).

In two dimensions, i.e. $\mathbf{Q} : \Omega \to \mathbb{R}^{2\times2}$, $\mathbf{Q}$ always has the form

$$\mathbf{Q} = s\left(\mathbf{n}\otimes\mathbf{n} - \tfrac{1}{2}\mathbf{I}\right), \tag{17}$$

where $\mathbf{n} : \Omega \to \mathbb{R}^2$, and $s \in [-1, 1]$.

2.2.2. Landau-deGennes energy

The LdG model seeks a minimizer $\mathbf{Q}$ of a free energy functional. Often, the one-constant model is used, which is stated in dimensional terms by [1,67,82]:

$$E_{\text{LdG,one}}[\mathbf{Q}] \quad := \tfrac{1}{2}\int_\Omega L_1|\nabla\mathbf{Q}|^2\, d\mathbf{x} + \int_\Omega \psi_{\text{LdG}}(\mathbf{Q})\, d\mathbf{x}, \tag{18}$$

where L_1 is a material parameter (on the order of 10^{-11} J/m [79, Table 1, pg. 168]), $|\nabla \mathbf{Q}|^2 := (\partial_k Q_{ij})(\partial_k Q_{ij})$ (we use the convention of summation over repeated indices), and ψ_{LdG} is a "bulk" (thermotropic) potential. More complicated energies can also be considered [1,67,82].

The bulk potential ψ_{LdG} is a double-well type of function that controls the eigenvalues of $\mathbf{Q}$, where the simplest form is given by

$$\psi_{\text{LdG}}(\mathbf{Q}) = K + \tfrac{A}{2}\text{tr}(\mathbf{Q}^2) - \tfrac{B}{3}\text{tr}(\mathbf{Q}^3) + \tfrac{C}{4}\left(\text{tr}(\mathbf{Q}^2)\right)^2, \tag{19}$$

where A, B, C are material parameters such that A has no sign, and B, C are positive; K is a convenient constant to ensure non-negativity of $\psi_{\text{LdG}}(\mathbf{Q})$. Usually, A is temperature dependent, e.g. $A = \alpha(T - T^*)$. Standard physical values for these parameters are approximately 10^5 J/m^3 [79, Table 1, pg. 168].

If A is bounded by a sufficiently small constant, then it is well-known [67] that the global minimizer $\mathbf{Q}^*$ of (19) has a *uniaxial* form. Thus, the double well functions (19) and (2) are connected in the following way. Assuming $\mathbf{Q}$ is uniaxial (15), we have the following calculations (in three dimensions)

$$\text{tr}(\mathbf{Q}^2) = \frac{2}{3}s^2, \quad \text{tr}(\mathbf{Q}^3) = \frac{2}{9}s^3. \tag{20}$$

Hence,

$$\psi_{\text{LdG}}(\mathbf{Q}) = K + \tfrac{A(2/3)}{2}s^2 - \tfrac{B(2/9)}{3}s^3 + \tfrac{C(4/9)}{4}s^4, \tag{21}$$

so then $A' = A(2/3)$, $B' = B(2/9)$, $C' = C(4/9)$. Typical choices of these parameters yield an asymmetric double-well function (in terms of s) with two local minimizers located at $s_- < 0$ and $s_+ > 0$ with s_+ being the global minimizer.

In two dimensions, the double-well has a modified form. For a uniaxial $\mathbf{Q}$ in $\mathbb{R}^2$, $\mathbf{Q}^2 = (s^2/4)\mathbf{I}$, thus $\text{tr}(\mathbf{Q}^2) = s^2/2$ and $\text{tr}(\mathbf{Q}^3) = 0$. Therefore, (21) becomes

$$\psi_{\text{LdG}}(\mathbf{Q}) = K + \tfrac{A/2}{2}s^2 + \tfrac{C/4}{4}s^4, \tag{22}$$

so then $A' = A/2, B' \equiv 0, C' = C/4$. Clearly, (22) is symmetric in s. Moreover, A must be negative to yield a double well with two symmetric global minimizers.

2.2.3. Non-dimensionalization

Following a similar approach in [80], we non-dimensionalize the energy in (18); note that $\mathbf{Q}$ is already non-dimensional. Let A_0 be the characteristic scale for the double well (19), and define $\eta_{\text{B}} := \sqrt{L_1/(A_0 R_0^2)}$, where $R_0 = \text{diam}(\Omega)$ is the length scale. Then, (18) becomes

$$\begin{aligned} E_{\text{LdG,one}}[\mathbf{Q}] &= L_1 R_0 \overline{E}_{\text{LdG,one}}[\mathbf{Q}], \\ \overline{E}_{\text{LdG,one}}[\mathbf{Q}] &= \int_\Omega |\nabla \mathbf{Q}|^2 \, d\mathbf{x} + \frac{1}{\eta_{\text{B}}^2}\overline{E}_{\text{b}}[\mathbf{Q}], \end{aligned} \tag{23}$$

$$\overline{E}_{\text{b}}[\mathbf{Q}] := \textstyle\int_\Omega \bar{\psi}_{\text{LdG}}(\mathbf{Q})\, d\mathbf{x}, \quad \bar{\psi}_{\text{LdG}}(\mathbf{Q}) = \frac{1}{A_0}\psi_{\text{LdG}}(\mathbf{Q}), \tag{24}$$

where $\bar{\psi}_{\text{LdG}}(\mathbf{Q})$, $\overline{\mathcal{W}}_{\text{LdG}}$, and $\overline{E}_{\text{b}}[\mathbf{Q}]$ are non-dimensional, as well as the domains. For the rest of the paper, we deal with $\overline{E}_{\text{LdG}}[\mathbf{Q}]$ and drop the "bar" from the non-dimensional quantities for simplicity (i.e. we ignore the pre-factor $L_1 R_0$ in $E_{\text{LdG}}[\mathbf{Q}]$).

2.2.4. Function space framework

We briefly review the function space setting of the LdG model, which is mostly standard; see [38] for more details. The function space for $\mathbf{Q}$ when seeking a minimizer is given by

$$V(\mathbf{G}) := \left\{\mathbf{Q} \in H^1(\Omega) \mid \mathbf{Q}(\mathbf{x}) \in \mathbf{\Lambda}, \forall \mathbf{x} \in \Omega, \ \mathbf{Q}|_\Gamma = \mathbf{G}\right\}, \tag{25}$$

where $\mathbf{G} \in H^1(\Omega)$ is arbitrary such that $\mathbf{G}(\mathbf{x}) \in \mathbf{\Lambda}$ for all $\mathbf{x} \in \Omega$.

The minimization problem for the Landau-deGennes free energy functional is as follows

$$\min_{\mathbf{Q} \in V(\mathbf{Q}_D)} E_{\text{LdG}}[\mathbf{Q}], \tag{26}$$

where $\mathbf{Q}_D \in H^1(\Omega)$ is given and $\mathbf{Q}_D(\mathbf{x}) \in \mathbf{\Lambda}$ for all $\mathbf{x} \in \Omega$. This minimization problem is not as delicate as (11); for instance, there is no non-convex constraint. Existence of a minimizer for (26) is guaranteed by standard elliptic PDE theory, i.e. from [38, Thm 6.3], we have the following result.

Theorem 8 (regularity). *Let Ω be a bounded, open, connected set, and assume Ω is either convex or $C^{1,1}$. Then any solution of (26) satisfies $\mathbf{Q} - \mathbf{Q}_D \in H^2(\Omega) \cap H_0^1(\Omega)$ provided $\mathbf{Q}_D \in H^2(\Omega)$.*

Remark 9 (uniaxial boundary conditions). It is typical to choose $\mathbf{Q}_D$ of the form $\mathbf{Q}_D = s^*(\boldsymbol{\nu} \otimes \boldsymbol{\nu} - \frac{1}{3}\mathbf{I})$, where $\boldsymbol{\nu} \equiv [\nu_k]_{k=1}^3$ is the unit outer normal of Γ, and s^* is the global min of ψ. We use this choice throughout.

2.3. The uniaxially constrained Landau-deGennes model

Many thermotropic LCs do *not* exhibit biaxiallity, i.e. they are purely uniaxial [67, Section 4.1]; indeed, only relatively recently was a biaxial thermotropic LC found [83–85]. However, minimizing the one-constant Landau-deGennes energy $E_{\text{LdG,one}}[\mathbf{Q}]$ (23) does not guarantee that the minimizer will be uniaxial (15); indeed, they may have a *biaxial escape*, especially near a defect [86–88]. Thus, the standard LdG model does not explicitly respect the structure of many common LC materials.

Therefore, we consider the so-called *uniaxially constrained* Landau-deGennes one-constant model. This constrained model has many similarities with the Ericksen model, yet it is still capable of modeling line fields and capturing half-integer defects.

2.3.1. Model derivation

For a uniaxially constrained $\mathbf{Q}$-tensor as in (15), we write $\mathbf{\Theta} = \mathbf{n} \otimes \mathbf{n}$, which will be treated as a control variable in minimizing (23). Define the set

$$L^{d-1} = \{\mathbf{A} \in \mathbb{R}^{d \times d} \ : \text{there exists } \mathbf{n} \in \mathbb{S}^{d-1}, \ \mathbf{A} = \mathbf{n} \otimes \mathbf{n}\}, \tag{27}$$

which can be identified with the real projective space $\mathbf{RP}^{d-1}$ through the map

$$\mathbf{n} \otimes \mathbf{n} \longmapsto \{\mathbf{n}, -\mathbf{n}\}.$$

Hence, the uniaxially constrained (LdG) model takes into account the molecular *direction* but not the orientation, so it does not have the same orientational bias as the Oseen-Frank and Ericksen models.

Taking d to be the dimension, recalling (15), (17), and noting $\nabla \mathbf{Q} = \nabla s \otimes (\mathbf{\Theta} - \frac{1}{d}\mathbf{I}) + s\nabla \mathbf{\Theta}$, we have

$$|\nabla \mathbf{Q}|^2 = |\nabla s|^2 \left|\mathbf{\Theta} - \frac{1}{d}\mathbf{I}\right|^2 + s^2|\nabla \mathbf{\Theta}|^2 + 2s\left[\nabla s \otimes \left(\mathbf{\Theta} - \frac{1}{d}\mathbf{I}\right)\right] : \nabla \mathbf{\Theta}.$$

Since $|\mathbf{\Theta} - \frac{1}{d}\mathbf{I}|^2 = \frac{d-1}{d}$ and $[\nabla s \otimes (\mathbf{\Theta} - \frac{1}{d}\mathbf{I}] : \nabla \mathbf{\Theta} = 0$, we get $|\nabla \mathbf{Q}|^2 = \frac{d-1}{d}|\nabla s|^2 + s^2|\nabla \mathbf{\Theta}|^2$. So enforcing the uniaxial constraint directly in (23) leads to the following (non-dimensionalized) energy functional

$$\begin{aligned} E_{\text{LdG,one}}[\mathbf{Q}] &= E_{\text{uni}}[s, \mathbf{\Theta}] = E_{\text{uni-m}}[s, \mathbf{\Theta}] + \frac{1}{\eta_{\text{B}}^2}E_{\text{dw}}[s], \\ E_{\text{uni-m}}[s, \mathbf{\Theta}] &:= \frac{1}{2}\left(\frac{d-1}{d}\int_\Omega |\nabla s|^2 \, dx + \int_\Omega s^2|\nabla \mathbf{\Theta}|^2 \, dx\right), \end{aligned} \tag{28}$$

which is the *exact same form* as (4), (5) except $\mathbf{\Theta}$ replaces $\mathbf{n}$ and b_0 replaces $(d-1)/d$.

2.3.2. Function space and boundary conditions

Following the same outline as in Section 2.1.3, we introduce a change of variable $\mathbf{U} = s\mathbf{\Theta}$ and rewrite

$$E_{\text{uni-m}}[s,\boldsymbol{\Theta}] = \widetilde{E}_{\text{uni-m}}[s,\mathbf{U}] := \frac{1}{2}\left(-\frac{1}{d}\int_\Omega |\nabla s|^2\,dx + \int_\Omega |\nabla \mathbf{U}|^2\,dx\right). \quad (29)$$

Hence, the admissible class is

$$\mathcal{A}_{\text{uni}} := \{(s,\boldsymbol{\Theta}) \in H^1(\Omega) \times [L^\infty(\Omega)]^{d\times d} : (s,\mathbf{U},\boldsymbol{\Theta}) \text{ satisfies (31), with } \mathbf{u} \in [H^1(\Omega)]^d\}, \quad (30)$$

with the structural condition

$$\mathbf{U} = s\boldsymbol{\Theta}, \quad -1/(d-1) \le s \le 1 \text{ a.e. in } \Omega, \text{ and } \boldsymbol{\Theta} \in L^{d-1} \text{ a.e. in } \Omega. \quad (31)$$

Moreover, we make similar assumptions on the boundary data as in Assumption 6.

Assumption 10 (Boundary Data is Regular)**.** There exists $g \in W^{1,\infty}(\mathbb{R}^d)$, $\mathbf{R} \in [W^{1,\infty}(\mathbb{R}^d)]^{d\times d}$, $\mathbf{M} \in [L^\infty(\mathbb{R}^d)]^{d\times d}$, such that ($g$, **R**, **M**) satisfies (31) on $\mathbb{R}^d$, i.e. $\mathbf{R} = g\mathbf{M}$ and $\mathbf{M} \in L^{d-1}$ a.e. in $\mathbb{R}^d$. Furthermore, we assume that g satisfies (9).

Therefore, the minimization problem is as follows

$$\min_{(s,\mathbf{n})\in\mathcal{A}_{\text{uni}}(g,\mathbf{M})} E_{\text{uni}}[s,\boldsymbol{\Theta}], \quad (32)$$

on the admissible class

$$\mathcal{A}_{\text{uni}}(g,\mathbf{M}) := \left\{(s,\mathbf{n}) \in \mathcal{A}_{\text{uni}} : \ s|_\Gamma = g, \quad \boldsymbol{\Theta}|_\Gamma = \mathbf{M}\right\}, \quad (33)$$

See [63,64] for more details on this constrained model.

3. Finite element discretization

We briefly describe the discretization approach to the Ericksen model in order to fully explain our domain decomposition approach in Section 4.2. More details about the discretization scheme can be found in [55,57]. Since the uniaxially constrained LdG model and Ericksen model are very similar, especially with regard to singularity of defects, we defer description of the discretization of (28) to [63,64] for more details.

3.1. Finite element spaces

We adopt an approach similar to [55, Sec. 2.2], except we discretize the Ericksen energy differently. First, approximate Ω by Ω_h which comes from a conforming shape regular triangulation $\mathcal{T}_h = \{T_i\}$ consisting of simplices. For simplicity, we assume that $\Omega \equiv \Omega_h$, i.e. there is no geometric error caused by the triangulation. Furthermore, let $\mathcal{N}_h$ be the set of nodes (vertices) of $\mathcal{T}_h$ and let N be the cardinality of $\mathcal{N}_h$ (with some abuse of notation).

Next, define continuous piecewise linear finite element spaces on Ω:

$$\begin{aligned} S_h &:= \{s_h \in H^1(\Omega) : s_h|_T \in \mathcal{P}_1(T), \forall T \in \mathcal{T}_h\}, \\ U_h &:= \{\mathbf{u}_h \in [H^1(\Omega)]^d : \mathbf{u}_h|_T \in \mathcal{P}_1(T), \forall T \in \mathcal{T}_h\}, \\ N_h &:= \{\mathbf{n}_h \in U_h : |\mathbf{n}_h(\mathbf{x}_i)| = 1, \forall \mathbf{x}_i \in \mathcal{N}_h\}, \end{aligned} \quad (34)$$

where the unit length constraint is enforced in N_h at the nodes (vertices) of the mesh. Dirichlet boundary conditions are included via the following discrete spaces:

$$\begin{aligned} S_h(g_h) &:= \{s_h \in S_h : s_h|_{\Gamma_s} = g_h\}, \\ U_h(\mathbf{r}_h) &:= \{\mathbf{u}_h \in U_h : \mathbf{u}_h|_{\Gamma_{\mathbf{u}}} = \mathbf{r}_h\}, \\ N_h(\mathbf{q}_h) &:= \{\mathbf{n}_h \in N_h : \mathbf{n}_h|_{\Gamma_{\mathbf{n}}} = \mathbf{q}_h\}, \end{aligned}$$

where $g_h := I_h g$, $\mathbf{r}_h := I_h \mathbf{r}$, and $\mathbf{q}_h := I_h \mathbf{q}$ is the discrete Dirichlet data. This leads to the following discrete admissible class with boundary conditions:

$$\mathcal{A}^h(g_h,\mathbf{q}_h) := \{(s_h,\mathbf{n}_h) \in S_h(g_h) \times N_h(\mathbf{q}_h) : (s_h,\mathbf{u}_h,\mathbf{n}_n) \text{ satisfies (36), with } \mathbf{u}_h \in U_h(\mathbf{r}_h)\}, \quad (35)$$

where

$$\mathbf{u}_h = I_h(s_h\mathbf{n}_h), \quad -1/2 \le s_h \le 1 \text{ in } \Omega, \quad \text{and } |\mathbf{n}_h(\mathbf{x}_i)| = 1, \forall \mathbf{x}_i \in \mathcal{N}_h, \quad (36)$$

is called the *discrete structural condition* of $\mathcal{A}^h$. If we write $(s_h, \mathbf{u}_h, \mathbf{n}_h)$ in $\mathcal{A}^h$, then this is equivalent to $(s_h, \mathbf{n}_h)$ in $\mathcal{A}^h$, $\mathbf{u}_h$ in U_h, and $(s_h, \mathbf{u}_h, \mathbf{n}_h)$ satisfies (36).

3.2. Discrete energy

The discretization of $E_s[s, \mathbf{n}]$ and $E_{\text{dw}}[s]$ is done in a standard way, i.e.

$$E_s^h[s_h,\mathbf{n}_h] := \frac{1}{2}\int_\Omega \left(b_0|\nabla s_h|^2 + s_h^2|\nabla \mathbf{n}_h|^2\right)d\mathbf{x}, \quad E_{\text{dw}}^h[s_h] := \int_\Omega \psi(s_h)\,d\mathbf{x}. \quad (37)$$

Remark 11. The energy $E_s^h[s_h,\mathbf{n}_h]$ is not the same as what was considered in [55]. An advantage of (37) is that it is more easily implemented with a standard finite element package than the energy in [55]. However, proving Γ-convergence is more involved but can be done by adapting the techniques in [58] and combining with the results in [55].

The term $\int_\Omega s_h^2|\nabla \mathbf{n}_h|^2\,d\mathbf{x}$ obeys a monotonicity property which will be useful in our minimization scheme (see Section 4.1). To better explain this, we introduce the standard piecewise linear "hat" function ϕ_i associated with a node $\mathbf{x}_i \in \mathcal{N}_h$ (i.e. $\{\phi_i\}$ are the basis functions of the spaces in (34)). Next, define the entries of the local (weighted) stiffness matrix corresponding to an element $T \in \mathcal{T}_h$:

$$\bar{k}_{ij}^T(s_h) := \int_T s_h^2\,\nabla\phi_i \cdot \nabla\phi_j\,d\mathbf{x}, \quad \text{for all nodes } i,j \text{ associated to } T. \quad (38)$$

If all elements in the mesh $\mathcal{T}_h$ are non-obtuse (i.e. interior angles $\le 90°$), then $\bar{k}_{ij}^T(s_h)$ satisfies the following property

$$\bar{k}_{ij}^T(s_h) \le 0, \quad \text{for all } i \ne j, \text{ for all } T \in \mathcal{T}_h. \quad (39)$$

Thus, defining $k_{ij}(s_h) := -\int_\Omega s_h^2 \nabla\phi_i \cdot \nabla\phi_j$, for all global indices i, j, then

$$k_{ij}(s_h) \ge 0, \quad \text{for all } i \ne j, \quad (40)$$

which follows by simply summing up the local stiffness matrices in the usual finite element methodology. Of course, requiring a non-obtuse mesh is a severe restriction, especially in three dimensions. However, the domains we consider allow for easy construction of non-obtuse meshes.

We can now derive an alternate form for $E_s^h[s_h,\mathbf{n}_h]$. Note that for all $\mathbf{x}_i \in \mathcal{N}_h$

$$\sum_{j=1}^N k_{ij}(s_h) = -\sum_{j=1}^N \int_\Omega s_h^2 \nabla\phi_i \cdot \nabla\phi_j\,dx = 0,$$

because $\sum_{j=1}^N \phi_j = 1$ in the domain Ω. So, if $S_h \ni w_h = \sum_{i=1}^N w_h(\mathbf{x}_i)\phi_i$, then

$$\int_\Omega s_h^2|\nabla w_h|^2 dx = -\sum_{i=1}^N k_{ii}(s_h)[w_h(\mathbf{x}_i)]^2 - \sum_{i,j=1,i\ne j}^N k_{ij}(s_h)w_h(\mathbf{x}_i)w_h(\mathbf{x}_j),$$

and using $k_{ii}(s_h) = -\sum_{j\ne i} k_{ij}(s_h)$ and the symmetry $k_{ij}(s_h) = k_{ji}(s_h)$, we get

$$\begin{aligned} \int_\Omega s_h^2|\nabla w_h|^2 dx &= \sum_{i,j=1}^N k_{ij}(s_h)w_h(\mathbf{x}_i)\big(w_h(\mathbf{x}_i) - w_h(\mathbf{x}_j)\big) \\ &= \frac{1}{2}\sum_{i,j=1}^N k_{ij}(s_h)\big(w_h(\mathbf{x}_i) - w_h(\mathbf{x}_j)\big)^2 \\ &= \frac{1}{2}\sum_{i,j=1}^N k_{ij}(s_h)\big(\delta_{ij}w_h\big)^2, \end{aligned} \quad (41)$$

where we define

$$\delta_{ij} w_h := w_h(\mathbf{x}_i) - w_h(\mathbf{x}_j), \quad \delta_{ij}\mathbf{w}_h := \mathbf{w}_h(\mathbf{x}_i) - \mathbf{w}_h(\mathbf{x}_j), \tag{42}$$

for any $w_h \in S_h$ and $\mathbf{w}_h \in U_h$. Thus, we can write $E_s^h[s_h, \mathbf{n}_h]$ as

$$E_s^h\big[s_h, \mathbf{n}_h\big] := \frac{1}{2}\int_\Omega b_0 |\nabla s_h|^2 \, d\mathbf{x} + \frac{1}{4}\sum_{i,j=1}^{N} k_{ij}(s_h)|\delta_{ij}\mathbf{n}_h|^2, \tag{43}$$

Writing the energy in this way leads to the following monotonicity result.

Proposition 12. *Suppose the mesh $\mathcal{T}_h$ is non-obtuse, namely (40) holds. Then, (43) has the following property:*

$$E_s^h\big[s_h, \mathbf{w}_h\big] \geq E_s^h\left[s_h, I_h\frac{\mathbf{w}_h}{|\mathbf{w}_h|}\right], \quad \text{for all } \mathbf{w}_h \in U_h. \tag{44}$$

Proof. The proof follows the same arguments as can be found in [51,55,89]. □

We need the following variational derivatives in Section 4.1:

$$\delta_{\mathbf{n}_h} E_s^h\big[s_h, \mathbf{w}_h; \mathbf{v}_h\big] = \int_\Omega s_h^2 \nabla \mathbf{w}_h \,:\, \nabla \mathbf{v}_h \, d\mathbf{x}, \tag{45}$$

$$\delta_{s_h} E_s^h\big[s_h, \mathbf{w}_h; z_h\big] = \int_\Omega \big(b_0 \nabla s_h \cdot \nabla z_h + s_h z_h |\nabla \mathbf{w}_h|^2\big) d\mathbf{x}, \tag{46}$$

which are defined for any s_h, $z_h \in S_h$, $\mathbf{w}_h$, $\mathbf{v}_h \in U_h$. Moreover, we use the following convex splitting of $\psi(s_h)$ [90,91]:

$$\begin{aligned} \psi_c(s_h) &= \frac{A' + D'}{2} s_h^2, \\ \psi_e(s_h) &= \frac{D'}{2} s_h^2 + \frac{B'}{3} s_h^3 - \frac{C'}{4} s_h^4 \;\Rightarrow\; \psi(s_h) \equiv \psi_c(s_h) - \psi_e(s_h), \end{aligned} \tag{47}$$

where $D' > 0$ is chosen sufficiently large, i.e. if $s_h \in [-1/2, 1]$, then ψ_c and ψ_e are both convex functions if $D' > 0$ is large enough. Hence, the variational derivative of the double well potential is given by

$$\delta_{s_h} E_{\text{dw}}^h[s_h; z_h] := \int_\Omega \psi'(s_h) z_h \, d\mathbf{x} = \int_\Omega \big(\psi_c'(s_h) - \psi_e'(s_h)\big) z_h d\mathbf{x}, \tag{48}$$

where, for time-stepping purposes, the s_h variable can be lagged in the ψ_e' term (see (52)).

4. Computing local minimizers

We begin by describing a robust, monotonically energy decreasing gradient flow scheme for the discrete Ericksen system (see [55,57]), followed by our domain decomposition (DD) approach that speeds up convergence by isolating defects. A heuristic explanation of the DD method is given in Section 4.3. A variant of this gradient flow scheme is used for the uniaxially constrained LdG model (28) (see [63,64] for more details).

4.1. Discrete gradient flow

We present a gradient descent type scheme for finding discrete (local) minimizers of $E_{\text{erk}}^h\big[s_h, \mathbf{n}_h\big]$; it is a variant of the minimization algorithms that can be found in [41,42,55,57]. To this end, because of the unit length constraint at the nodes in N_h (see (34)), we introduce the space of discrete tangential variations:

$$U_h^\perp(\mathbf{n}_h) = \{\mathbf{v}_h \in U_h \,:\, \mathbf{v}_h(x_i) \cdot \mathbf{n}_h(x_i) = 0 \text{ for all nodes } x_i \in \mathcal{N}_h\}, \tag{49}$$

as well as an effective inner product $a_{\mathbf{n}}(\,\cdot\,,\,\cdot\,)$ on $U_h^\perp(\mathbf{n}_h)$ and an inner product $a_s(\,\cdot\,,\,\cdot\,)$ on S_h.

Algorithm 1 Gradient flow algorithm for the Ericksen model.

Set $\delta t > 0$. Given $(s_h^0, \mathbf{n}_h^0)$ in $S_h(g_h) \times N_h(\mathbf{q}_h)$,iterate steps (1)-(2) for $k \geq 0$.

1. Descent for $\mathbf{n}_h$.
   (a) Tangent update. Find $\mathbf{t}_h^{k+1} \in U_h^\perp(\mathbf{n}_h^k) \cap H_\Gamma^1(\Omega)$ such that, for all $\mathbf{v}_h \in U_h^\perp(\mathbf{n}_h^k) \cap H_\Gamma^1(\Omega)$, we have (see (45))
   $$a_{\mathbf{n}}\big(\mathbf{t}_h^{k+1}, \mathbf{v}_h\big) = -\delta_{\mathbf{n}_h} E_{\text{erk}}^h\big[s_h^k, \tilde{\mathbf{n}}_h^{k+1}; \mathbf{v}_h\big], \quad \tilde{\mathbf{n}}_h^{k+1} := \mathbf{n}_h^k + \mathbf{t}_h^{k+1}. \tag{50}$$
   (b) Normalization. Update $\mathbf{n}_h^k$ to $\mathbf{n}_h^{k+1}$ via
   $$\mathbf{n}_i^{k+1} := \frac{\mathbf{n}_i^k + \mathbf{t}_i^{k+1}}{|\mathbf{n}_i^k + \mathbf{t}_i^{k+1}|}, \quad \text{at all nodes } x_i \in \mathcal{N}_h. \tag{51}$$
2. Gradient descent for s_h. Find $s_h^{k+1} \in S_h(g_h)$ such that, for all $z_h \in S_h \cap H_\Gamma^1(\Omega)$, we have (see (46) and (48))
   $$a_s\left(\frac{s_h^{k+1} - s_h^k}{\delta t}, z_h\right) = -\delta_{s_h} E_{\text{erk}}^h\big[s_h^{k+1}, \mathbf{n}_h^{k+1}; z_h\big]. \tag{52}$$

The algorithm terminates when the change in the energy $E_{\text{erk}}^h\big[s_h, \mathbf{n}_h\big]$ is below a certain tolerance.

The minimization scheme for $E_{\text{erk}}^h[s_h, \mathbf{n}_h]$ is an alternating direction, semi-implicit method, where energy decreasing steps are taken with respect to $\mathbf{n}_h$ and s_h consecutively. The following result guarantees that this scheme is energy decreasing.

Theorem 13 (energy decrease). *Suppose the mesh $\mathcal{T}_h$ is non-obtuse, namely (40) holds. Then, for any $\delta t > 0$, the iterate $(s_h^{k+1}, \mathbf{n}_h^{k+1})$ of Algorithm 1 exists and satisfies*

$$E_{\text{erk}}^h\big[s_h^{k+1}, \mathbf{n}_h^{k+1}\big] \leq E_{\text{erk}}^h\big[s_h^k, \mathbf{n}_h^k\big] - \frac{1}{\delta t} a_s\big(s_h^{k+1} - s_h^k, s_h^{k+1} - s_h^k\big). \tag{53}$$

Equality holds if and only if $(s_h^{k+1}, \mathbf{n}_h^{k+1}) = (s_h^k, \mathbf{n}_h^k)$ (a local minimizer).

Proof. The proof follows a similar argument as in [55, Thm. 4.2]. □

4.2. Domain decomposition approach

We describe an alternating Schwarz method, with overlapping subdomains, for enhancing the gradient flow scheme in Section 4.1. Our focus is on a small number of sub-domains, say two, but we present it for any number of sub-domains, say M. Let $\{\Omega_i^*\}_{i=1}^M$ be an *overlapping decomposition* of Ω, i.e. $\cup_{i=1}^M \Omega_i^* = \Omega$ where each Ω_i^* is an open subset of Ω. Moreover, we define the sub-domain boundaries $\Gamma_i := \partial\Omega_i^*$.

Next, define $\mathcal{K}_i^k\big[(s_h, \mathbf{n}_h)\big]$ to be k iterations of Algorithm 1, with initial guess $(s_h, \mathbf{n}_h)$, but restricted to sub-domain Ω_i^*. In other words, we replace Ω with Ω_i^* in the gradient flow, and impose boundary conditions on Γ_i, whose boundary values are given by the initial guess: $(s_h, \mathbf{n}_h)$ restricted to Γ_i. Moreover, $\mathcal{K}^k\big[(s_h, \mathbf{n}_h)\big]$ denotes the gradient flow algorithm on Ω with boundary conditions imposed on Γ. *The variable sub-domain Schwarz method* we consider is the following.

Remark 14. If the sub-domains are fixed throughout all iterations, and if $k_i = \infty$, for $i = 1, ..., M$, then Algorithm 2 becomes the classic continuous Schwarz alternating method, where each sub-problem is solved exactly.

The main purpose of introducing this domain decomposition (DD) method is to isolate regions that contain defects, i.e. the singular set (3). Numerical experience shows that the speed of the (weighted) gradient flow is dictated by the motion of defects. Therefore, the procedure for determining the sub-domains is based on s_h^l (the degree of orientation parameter). The first sub-domain captures the singular region and the remaining sub-domains simply partition the "regular" region.

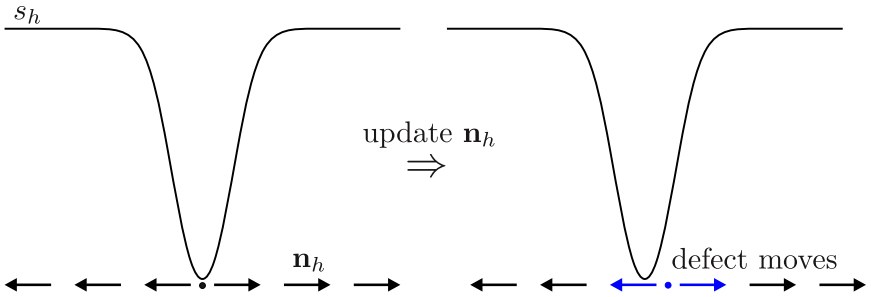

Fig. 1. Illustration of how defects impede gradient flow scheme in Algorithm 1 (one dimensional example). The presence of a defect tightly couples $\mathbf{n}_h$ and s_h. Since they are updated in separate steps, updating $\mathbf{n}_h$ is limited by s_h and vice-versa (see blue arrows).

Algorithm 2 Alternating Schwarz method for the Ericksen model.

Set integers $k_1, k_2, ..., k_M > 0$. Given $(s_h, \mathbf{n}_h)^0 \equiv (s_h^0, \mathbf{n}_h^0)$ in $S_h(g_h) \times N_h(\mathbf{q}_h)$, iterate the following procedure for $l \geq 0$:

1. Determine an overlapping sub-domain decomposition $\{\Omega_i^*\}_{i=1}^M$ from s_h^l using (56). Note that we suppress the dependence of $\{\Omega_i^*\}_{i=1}^M$ on l.
2. For $i = 1, 2, ..., M$ do:
   (a) Let $(\bar{s}_h, \bar{\mathbf{n}}_h)^{l+\frac{i}{M}} := \mathcal{K}_i^{k_i}\left[(s_h, \mathbf{n}_h)^{l+\frac{i-1}{M}}\right]$, i.e. run the sub-domain gradient flow.
   (b) Update:

$$(s_h, \mathbf{n}_h)^{l+\frac{i}{M}} := \begin{cases} (\bar{s}_h, \bar{\mathbf{n}}_h)^{l+\frac{i}{M}}, & \text{on } \overline{\Omega_i^*}, \\ (s_h, \mathbf{n}_h)^{l+\frac{i-1}{M}}, & \text{on } \Omega \setminus \overline{\Omega_i^*}. \end{cases} \tag{54}$$

3. Goto 1.

Define the following general sets of nodes in terms of s_h

$$\begin{aligned} \mathcal{S}_h(a,b) &:= \{\mathbf{x}_i \in \mathcal{N}_h \mid a \leq |s_h(\mathbf{x}_i)| \leq b\}, \\ \mathcal{Z}_h(a,b,r) &:= \{\mathbf{x}_i \in \mathcal{N}_h \mid \operatorname{dist}(\mathbf{x}_i, \mathcal{S}_h(a,b)) \leq r\}, \end{aligned} \tag{55}$$

where $b > a \geq 0$, $r \geq 0$, and consider the following two domain decomposition ($M = 2$):

$$\begin{aligned} \mathcal{N}_{h,1} &:= \mathcal{Z}_h(a_1, b_1, r_1) \cup \{\mathbf{x}_i \in \mathcal{N}_h \mid s_h \text{ changes sign on some } T \ni \mathbf{x}_i\}, \\ \mathcal{N}_{h,2} &:= \mathcal{Z}_h(a_2, b_2, r_2), \\ \Omega_j^* &:= \{T \in \mathcal{T}_h \mid T \text{ contains a point } \mathbf{x}_i \in \mathcal{N}_{h,j}\}, \text{ for } j = 1, 2, \end{aligned} \tag{56}$$

where the constants $a_1, a_2, b_1, b_2, r_1, r_2$ are chosen to ensure Ω_1^*, Ω_2^* are non-empty, and have some overlap. Basically, we choose the constants so that Ω_1^*, which contains the defect region, is much smaller than Ω_2^*. In Section 5, we explore different choices of these constants.

The iteration numbers k_1, k_2 are chosen to reduce the overall computing time. Since Ω_1^* is a region much smaller than Ω_2^*, k_1 can be much larger than k_2 and still allow Step 2(a) of Algorithm 2 to take the same amount of time for each sub-domain. *The advantage of this* is that applying more iterations in the singular region ensures the defect will move closer to its equilibrium position, than with the standard (non-DD) approach, for the same computational effort. In Section 5, we explore different choices for k_1 and k_2.

Remark 15. A variant of the gradient flow scheme, Algorithm 1, is used for the uniaxially constrained LdG model (28) (see [63,64] for more details). Moreover, the DD approach for (28) is exactly the same, since it is based on the degree of orientation parameter s_h which has the same meaning in both models.

4.3. Heuristic explanation for speedup

Fig. 1 illustrates why the gradient flow scheme may perform slowly (for simplicity, we consider the problem in one dimension). If the director field $\mathbf{n}_h$ is forced to have a defect because of boundary conditions, then s_h will develop a degenerate region in one or two iterations (see left side of Fig. 1), because the scheme is energy decreasing. However, during subsequent iterations, the $\mathbf{n}_h$ and s_h variables are *tightly coupled* near the defect. In other words, when computing Step 1(a) of Algorithm 1, s_h is held fixed, which means the discontinuity in $\mathbf{n}_h$ (the defect) cannot move *too far* from where s_h is nearly zero. This is because the term $\int_\Omega s_h^2 |\nabla \mathbf{n}_h|^2 \, dx$ in the energy would be very large if the defect had moved to a region where s_h is well away from zero. Since the scheme is energy decreasing, this cannot happen. Similarly, when computing Step 2 of Algorithm 1, $\mathbf{n}_h$ is held fixed, which means that the degenerate region of s_h cannot move far from the defect in $\mathbf{n}_h$. We emphasize that this issue is exacerbated when the mesh size decreases because the term $\int_\Omega s_h^2 |\nabla \mathbf{n}_h|^2 \, dx$ is more singular.

Clearly, updating $\mathbf{n}_h$ and s_h *separately* is not optimal in terms of convergence rate to a minimizer. However, the gradient flow scheme is extremely robust, which is a feature we would like to preserve given the non-linear, non-convex, and degenerate nature of the models. This is what inspired the DD approach in Section 4.2. It is clear that the tight coupling is only present in a relatively small region surrounding the defect. So it is natural to use more iterations of the gradient flow in the "small" sub-domain containing the defect in order to move the defect further along toward a minimizer. Our numerical experiments in Section 5 validate this intuition.

Remark 16. If there is no defect present in the problem, then the gradient flow scheme performs efficiently. For smooth solutions, the scheme converges to a minimizer in about 10 to 15 iterations. This is because we use weighted (e.g. $H^1(\Omega)$) inner products for the gradient flow, which act as effective "pre-conditioners" that eliminate any "stiffness" when solving the linear systems. Thus, no additional acceleration is necessary in this case.

However, a weighted gradient flow (a linear concept) *cannot* remove the stiffness induced by defects because of their non-linear and degenerate nature. Other techniques, such as Newton's method, are also problematic because the solutions are not smooth; even with finite h, one must provide an extremely good initial guess to have any hope of convergence.

5. Numerical results

We explore the DD approach of Section 4.2 for both the Ericksen model and the uniaxially constrained **Q**-tensor model. The examples we use all exhibit defects of differing types. In particular, we illustrate the DD approach for different choices of sub-domain size and iteration count.

We implemented our method using the Matlab/C++ finite element toolbox FELICITY [92]. For all 3-D simulations, we used the algebraic multi-grid solver (AGMG) [93–96] to solve the linear systems for updating $\mathbf{n}_h$ and s_h. In 2-D, we simply used the "backslash" command in Matlab.

In all experiments, Ω_1^* contains the singular region. After some experimentation, we found that it was best to choose $\Omega_2^* \equiv \Omega$ and set $k_2 \equiv 1$, i.e. for each outer iteration of the gradient flow, we solve in the singular

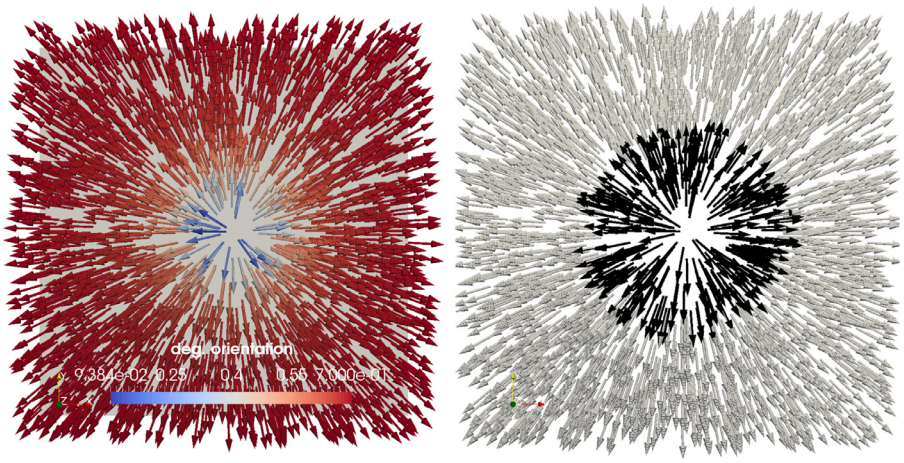

Fig. 2. Point defect at its equilibrium state (Section 5.2.1). Left: director $\mathbf{n}$ is shown colored according to the degree of orientation s; the minimum value of s is 9.384×10^{-2}. Right: a view of the sub-domain Ω_1^* in black.

region Ω_1^* several times, followed by one solve over the entire domain. Furthermore, in all cases (except Section 5.3.2), we first run 10 iterations of the standard gradient flow scheme over the entire domain so that the s variable can be used to identify the singular region. For each experiment, we list the inner products $a_{\mathbf{n}}(\cdot\,,\,\cdot)$ and $a_s(\cdot\,,\,\cdot)$ used in Algorithm 1.

In measuring the convergence performance, we use the scalar s variable, and $\mathbf{u} = s\mathbf{n}$ for the Ericksen model (recall (8)) and $\mathbf{U} = s\boldsymbol{\Theta}$ for the uniaxial LdG model (recall (31)). Using $\mathbf{n}$ (or $\boldsymbol{\Theta}$) is not appropriate because they are not very regular.

5.1. Choice of double well

In two and three dimensions ($d = 2, 3$), the double well potential satisfies

$$s^* \approx 0.7, \quad \psi(s^*) = 0, \quad \psi(0) = 1, \quad \psi(s) \propto s^4, \text{ for } s \to -1/(d-1), +1. \tag{57}$$

For numerical convenience, we do not modify ψ to diverge at $s = -1/(d-1), +1$; none of the simulations ever exhibited s_h near the physical bounds, so this is acceptable.

In two dimensions, the double-well potential, with convex splitting, is given by

$$\begin{aligned}\psi(s) &= \psi_c(s) - \psi_e(s) \\ &:= (26.20577s^2 + 1) - (-4.1649313s^4 + 30.2874s^2).\end{aligned}$$

In three dimensions, the double-well potential is given by

$$\begin{aligned}\psi(s) &= \psi_c(s) - \psi_e(s) \\ &:= (36.7709s^2 + 1) - (-7.39101s^4 + 4.51673s^3 + 39.27161s^2).\end{aligned}$$

5.2. The Ericksen model

5.2.1. A point defect in 2-D

We simulate a point defect moving to the center of the domain (Ω is the unit square). The time-step is $\delta t = 1.0$, the maximum mesh size is $h = 0.00913533$, and the inner products are $a_{\mathbf{n}}(\mathbf{n}, \mathbf{v}) = (\mathbf{n}, \mathbf{v}) + 0.5\big((s^k)^2\nabla\mathbf{n}, \nabla\mathbf{v}\big)$ (where s^k is known), and $a_s(s, z) = (s, z) + 0.5(\nabla s, \nabla z)$. We set $b_0 = 1$, $\epsilon_{\text{dw}} = 0.2$, and impose the following Dirichlet boundary conditions for s and $\mathbf{n}$

$$s = s^*, \quad \mathbf{n} = \frac{(x, y) - (0.5, 0.5)}{|(x, y) - (0.5, 0.5)|}, \quad \text{on } \Gamma := \partial\Omega. \tag{58}$$

Initial conditions on Ω for the gradient flow are: $s = s^*$ and a point defect located at (0.7167,0.2912). Fig. 2 depicts the equilibrium solution.

Table 1
Error (in ℓ_∞) between the final result with 0 iterations and 4, 8 iterations, respectively (Section 5.2.1).

	Iter 4 (A)	Iter 4 (B)	Iter 8 (A)	Iter 8 (B)
s	2.541928E-07	2.541928E-07	2.541928E-07	2.541928E-07
$\mathbf{u}$	2.859279E-07	2.859279E-07	2.859279E-07	2.859279E-07

Fig. 3 shows the convergence to equilibrium versus the run-time for different choices of the parameters in the DD approach. The singular sub-domain Ω_1^* is defined by

$$a_1 = 0, \quad b_1 = 0.1, \quad \text{and } r_1 = 0.2, \text{ or } 0.3. \tag{59}$$

The number of (inner) iterations used in Ω_1^* was $k_1 = 0$, 4, or 8. Convergence for each iteration case (0, 4, 8) was measured with respect to the final result for that case. Table 1 shows the error between the final result of the 0 iteration case and the final results of the 4 and 8 iteration cases. The DD approach shows a clear speed-up.

5.2.2. A saturn-ring like defect in 3-D

The domain Ω is taken to be a long rectangular "tube" (vertically oriented) with a spherical hole at its center (see [57] for a full description of the domain). The boundary of Ω partitions into two disjoint connected pieces $\partial\Omega = \Gamma_i \cup \Gamma_o$, where Γ_o is the outer part of the tube, and Γ_i is the boundary of the inner spherical hole.

The time-step is $\delta t = 1.0$, the mesh size is $h = 0.0785036$, and the inner products are $a_{\mathbf{n}}(\mathbf{n}, \mathbf{v}) = (\mathbf{n}, \mathbf{v}) + 0.5\big((s^k)^2\nabla\mathbf{n}, \nabla\mathbf{v}\big)$ (where s^k is known), and $a_s(s, z) = (s, z) + 0.5(\nabla s, \nabla z)$. We set $b_0 = 1$, $\epsilon_{\text{dw}} = 0.3$, and impose the following Dirichlet boundary conditions

$$\mathbf{n} = \boldsymbol{\nu}, \text{ on } \Gamma_i, \quad s = s^*, \text{ on } \partial\Omega, \tag{60}$$

and $\mathbf{n}$ smoothly interpolates between $(0, 0, -1)^T$ and $(0, 0, 1)^T$ on Γ_o. The initial conditions in Ω for the gradient flow are: $s = s^*$ and

$$\mathbf{n}(x, y, z) = (0, 0, -1)^T, \quad \text{if } z < 0,$$
$$\mathbf{n}(x, y, z) = (0, 0, +1)^T, \quad \text{if } z \geq 0.$$

Fig. 4 depicts the equilibrium solution.

Fig. 5 shows the convergence to equilibrium versus the run-time for different choices of the parameters in the DD approach. The singular sub-domain Ω_1^* is defined by

$$a_1 = 0, \quad b_1 = 0.25, \quad \text{and } r_1 = 0.25, \text{ or } 0.5. \tag{61}$$

The number of (inner) iterations used in Ω_1^* was $k_1 = 0$, 4, or 8. Convergence for each iteration case (0, 4, 8) was measured with respect to the final result for that case. Table 2 shows the error between the final result of the 0 iteration case and the final results of the 4 and 8 iteration

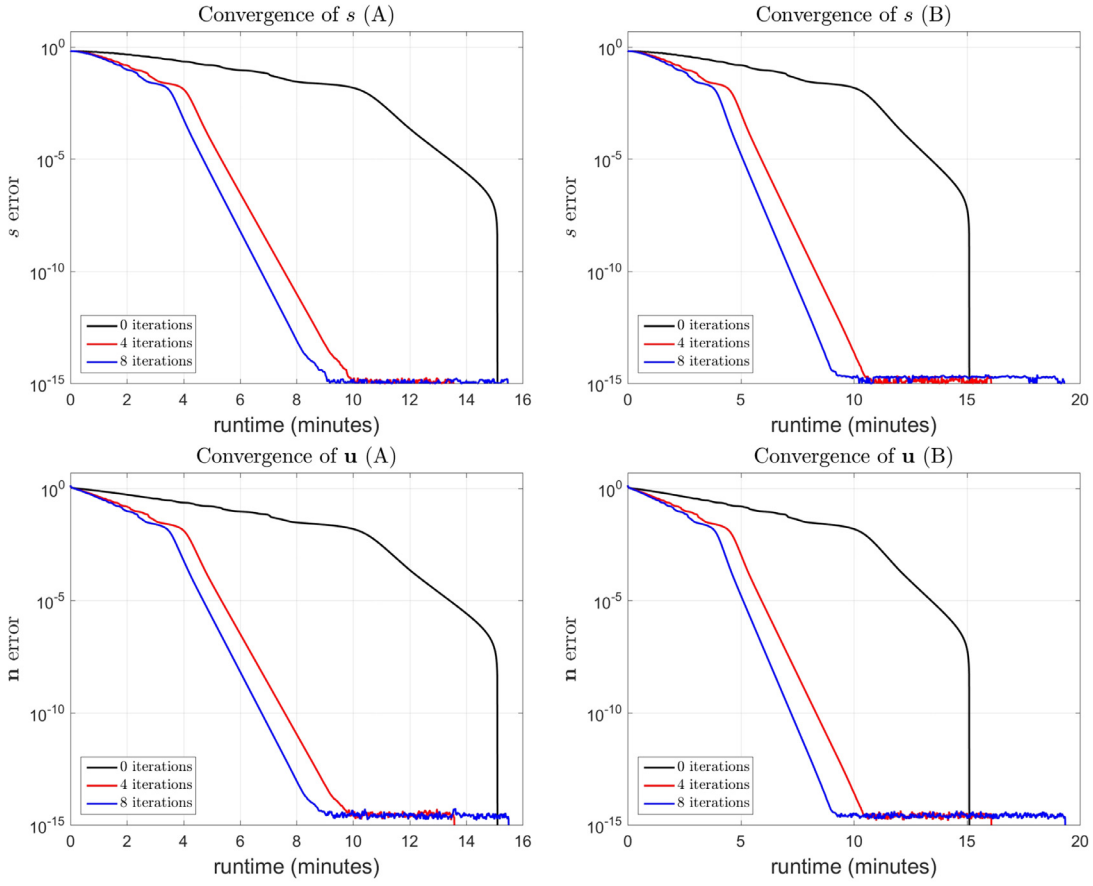

Fig. 3. Ericksen point defect convergence results for s and $\mathbf{u}$ (Section 5.2.1) using the ℓ_∞ norm of the error. Plot (A) corresponds to $r_1 = 0.2$; Plot (B) corresponds to $r_1 = 0.3$. Number of iterations is for the singular sub-domain Ω_1^*.

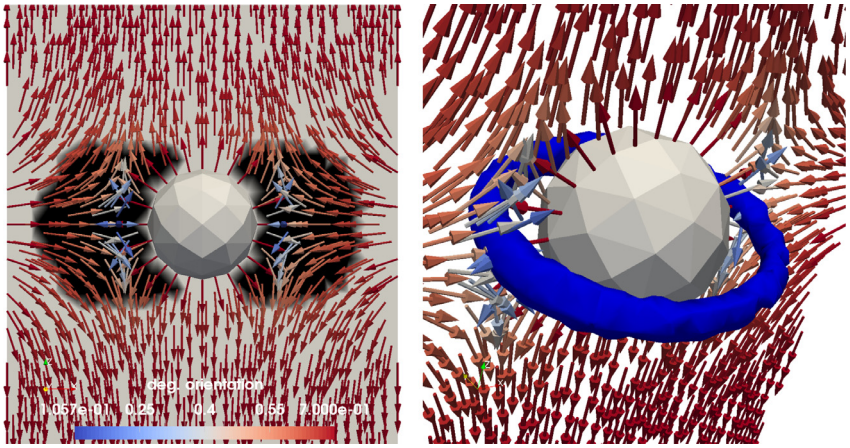

Fig. 4. Ericksen version of the Saturn ring defect at its equilibrium state (Section 5.2.2). Left: director $\mathbf{n}$ is shown on a vertical slice through Ω colored according to the degree of orientation s; the minimum value of s is 0.1057. The spherical inclusion is shown and the sub-domain Ω_1^* is depicted in black. Right: an oblique view of the same vertical slice with the $s = 0.2$ iso-surface shown.

Table 2
Error (in ℓ_∞) between the final result with 0 iterations and 4, 8 iterations, respectively (Section 5.2.2).

	Iter 4 (A)	Iter 4 (B)	Iter 8 (A)	Iter 8 (B)
s	1.450184E-05	1.451180E-05	0.071109	1.450584E-05
$\mathbf{u}$	4.153856E-05	4.156694E-05	0.167288	4.155104E-05

cases. The DD approach achieves some speed-up here over the standard method, but not as dramatic as in Section 5.2.1. Moreover, Table 2 indicates that a different minimizer was found for the case of 8 sub-iterations with $r_1 = 0.25$ (A). Note that the minimization problem (11) is not convex; indeed, LC problems typically exhibit multiple minima.

5.3. The uniaxially constrained **Q**-Model

5.3.1. A +1/2 defect in 2-D

We simulate a +1/2 degree defect moving to the center of the domain (Ω is the unit square). The time-step is $\delta t = 0.01$, the mesh size is $h = 0.00913533$, and the inner products are $a_{\mathbf{n}}(\mathbf{n}, \mathbf{v}) = (\mathbf{n}, \mathbf{v}) + 0.5\big((s^k)^2 \nabla \mathbf{n}, \nabla \mathbf{v}\big)$ (where s^k is known), and $a_s(s, z) = (s, z) + 0.5(\nabla s, \nabla z)$. We set $b_0 = (d-1)/d = 1/2$, $\eta_B = 0.25$, and impose the following Dirich-

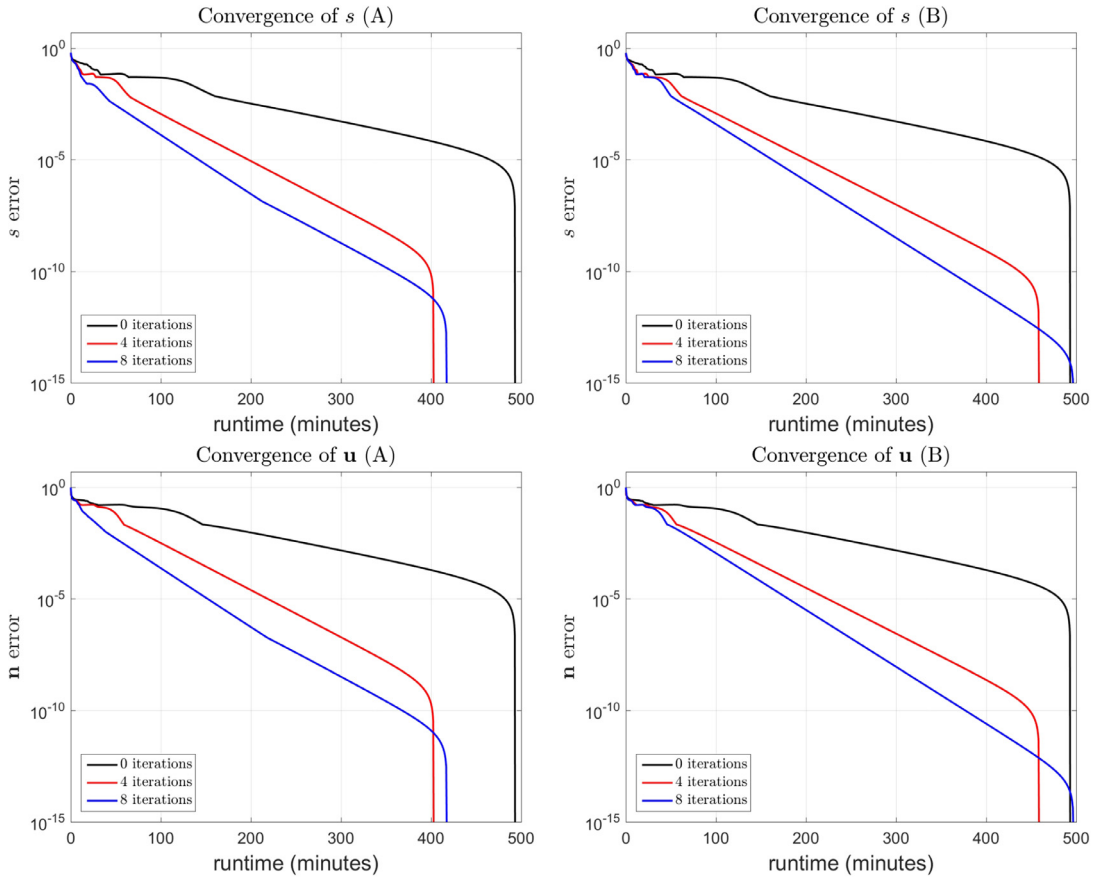

Fig. 5. Ericksen Saturn ring defect convergence results for s and $\mathbf{u}$ (Section 5.2.2) using the ℓ_∞ norm of the error. Plot (A) corresponds to $r_1 = 0.25$; Plot (B) corresponds to $r_1 = 0.5$. Number of iterations is for the singular sub-domain Ω_1^*.

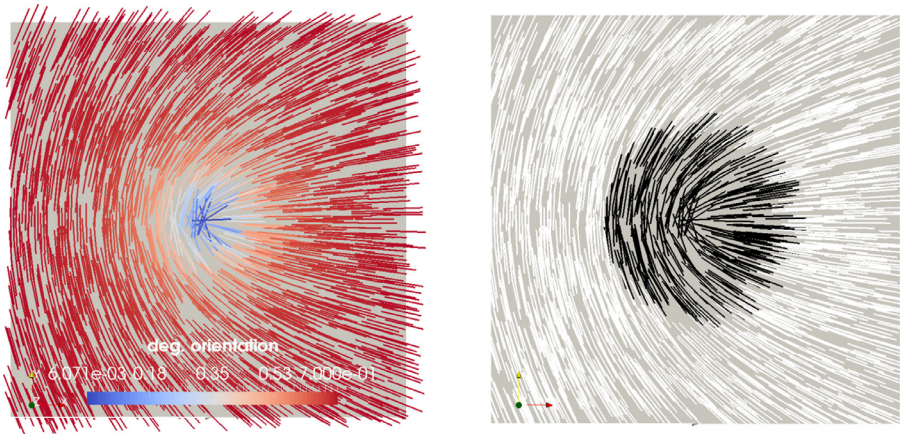

Fig. 6. A $+1/2$ degree defect at its equilibrium state (Section 5.3.1). Left: director $\mathbf{n}$ (as a line-field) is shown colored according to the degree of orientation s; the minimum value of s is 6.071×10^{-3}. Right: a view of the sub-domain Ω_1^* in black.

let boundary conditions for s and $\mathbf{n}$

$$s = s^*, \quad \mathbf{n}(x, y) = (\cos\theta, \sin\theta)^\top,$$
$$\theta(x, y) = (1/2)\,\widetilde{\arctan}(x - 0.5, y - 0.5), \text{ on } \Gamma := \partial\Omega, \tag{62}$$

where $\widetilde{\arctan} : \mathbb{R}^2 \setminus \{0\} \to [-\pi, \pi]$ is the four quadrant inverse tangent function. Initial conditions on Ω for the gradient flow are: $s = s^*$ and a $+1/2$ degree defect located at (0.7167,0.2912). Fig. 6 depicts the equilibrium solution.

Fig. 7 shows the convergence to equilibrium versus the run-time for different choices of the parameters in the DD approach. The singular sub-domain Ω_1^* is defined by

$$a_1 = 0, \quad b_1 = 0.1, \quad \text{and } r_1 = 0.2, \text{ or } 0.3. \tag{63}$$

Table 3
Error (in ℓ_∞) between the final result with 0 iterations and 4, 8 iterations, respectively (Section 5.3.1).

	Iter 4 (A)	Iter 4 (B)	Iter 8 (A)	Iter 8 (B)
s	0.00561450	0.00501270	0.00574467	0.00497920
$\mathbf{U}$	0.00491533	0.00445426	0.00505201	0.00459453

The number of (inner) iterations used in Ω_1^* was $k_1 = 0$, 4, or 8. Convergence for each iteration case (0, 4, 8) was measured with respect to the final result for that case. Table 3 shows the error between the final

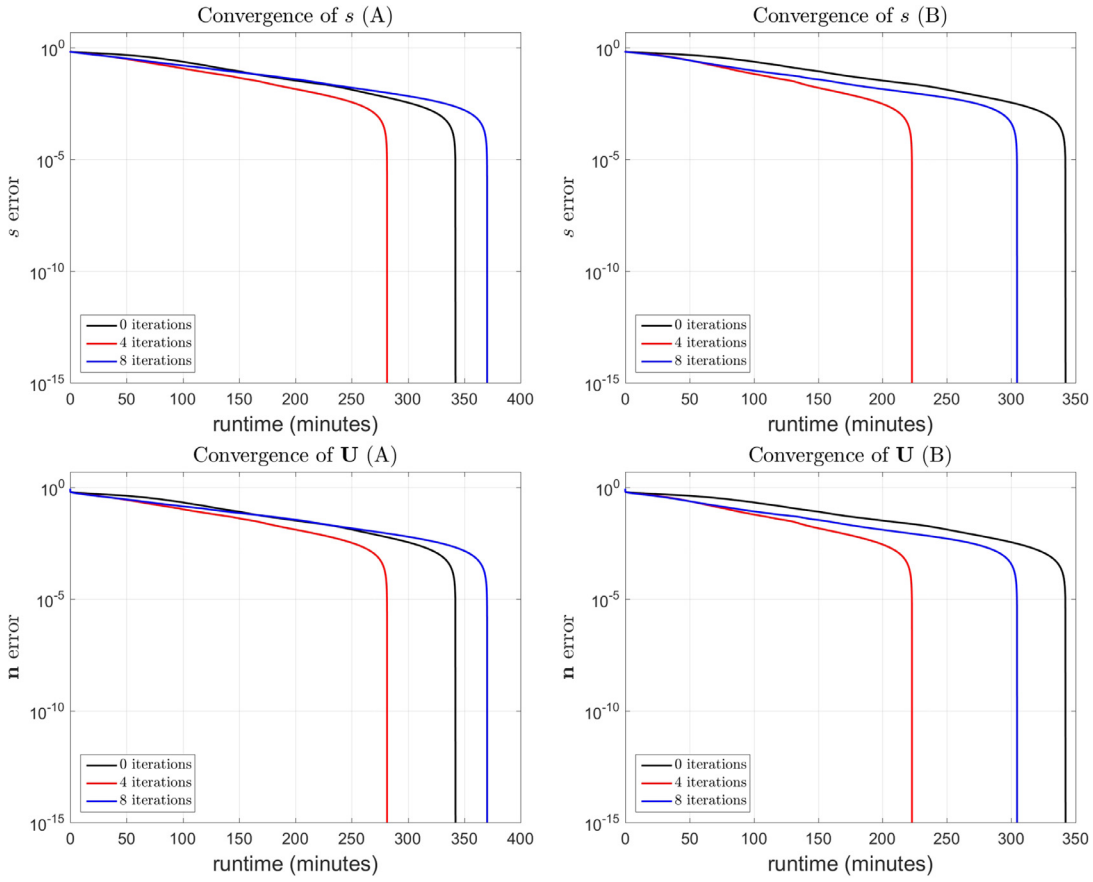

Fig. 7. Uniaxial LdG +1/2 degree defect convergence results for s and $\mathbf{U}$ (Section 5.3.1) using the ℓ_∞ norm of the error. Plot (A) corresponds to $r_1 = 0.2$; Plot (B) corresponds to $r_1 = 0.3$. Number of iterations is for the singular sub-domain Ω_1^*.

result of the 0 iteration case and the final results of the 4 and 8 iteration cases. The DD approach achieves some speed-up here over the standard method, but not as dramatic as in Section 5.2.1. Moreover, the errors in Table 3 indicate that the converged solutions are close, but not exact. Furthermore, Fig. 7 indicates that using fewer sub-iterations, but a larger sub-domain, gives better performance (contrary to Fig. 3).

5.3.2. The Saturn-ring defect in 3-D

The domain Ω is the same as in Section 5.2.2. The time-step is $\delta t = 0.001$, the mesh size is $h = 0.0785036$, and the inner products are $a_{\mathbf{n}}(\mathbf{n}, \mathbf{v}) = \left((s^k)^2 \nabla \mathbf{n}, \nabla \mathbf{v}\right)$ (where s^k is known), and $a_s(s, z) = (s, z) + (\nabla s, \nabla z)$. We set $b_0 = (d-1)/d = 2/3$, $\eta_B = 0.3$, and impose the following Dirichlet boundary conditions

$$\mathbf{n} = \boldsymbol{\nu}, \text{ on } \Gamma_i, \quad \mathbf{n} = (0,0,1)^T, \text{ on } \Gamma_o, \quad s = s^*, \text{ on } \partial\Omega. \tag{64}$$

The initial conditions in Ω for the gradient flow are: $s = s^*$ and $\mathbf{n} = (0,0,1)^T$.

The equilibrium solution is shown in Fig. 8. The structure of the director field is not the same as in Fig. 4; this is a consequence of the director being non-orientable. In Fig. 8, the cross-section of the director (line) field over the defect region clearly exhibits a $-1/2$ degree point defect, which is consistent with experimental evidence [97] of the Saturn-ring; see [98] for an analytical solution.

Fig. 9 shows the convergence to equilibrium versus the run-time for different choices of the parameters in the DD approach. The singular sub-domain Ω_1^* is defined by

$$a_1 = 0, \quad b_1 = 0.25, \quad \text{and } r_1 = 0.25, \text{ or } 0.5. \tag{65}$$

The number of (inner) iterations used in Ω_1^* was $k_1 = 0$, 4, or 8. Convergence for each iteration case (0, 4, 8) was measured with respect to the final result for that case. Table 4 shows the error between the final result of the 0 iteration case and the final results of the 4 and 8 iteration cases. The DD approach achieves some speed-up here over the standard method, but not as dramatic as in Section 5.2.1. Moreover, the errors in Table 3 indicate that the converged solutions are close, but not exact. Using a larger sub-domain appears to give a solution that is a better match. This could also be due to the fact that the minimization problem (32) is not convex, thus exhibiting multiple minima.

Table 4
Error (in ℓ_∞) between the final result with 0 iterations and 4, 8 iterations, respectively (Section 5.3.2).

	Iter 4 (A)	Iter 4 (B)	Iter 8 (A)	Iter 8 (B)
s	0.0128284	0.000379576	0.0161736	0.000596018
$\mathbf{U}$	0.0128879	0.00220264	0.0178509	0.00392691

6. Conclusions

We presented a domain decomposition approach to accelerate gradient flow schemes for a special class of degenerate elliptic models of liquid crystal equilibrium states. The key idea is to apply more gradient flow steps in a small region that contains the degenerate part of the solution, which is computationally cheaper than updating the solution over the entire domain. We emphasize that applying Newton's method to these degenerate models is not at all robust. Indeed, the initial guess for a Newton solver must be extremely close to the solution, which is never the case in practice.

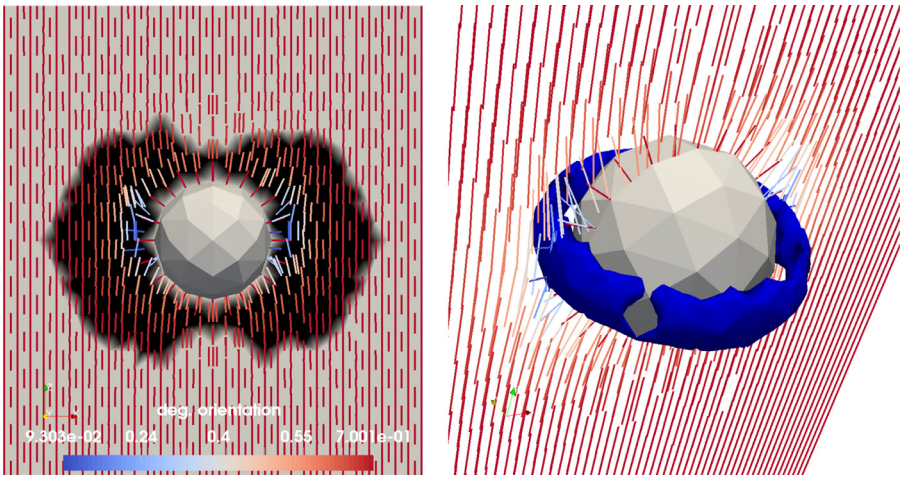

Fig. 8. Uniaxial LdG version of the Saturn ring defect at its equilibrium state (Section 5.3.2). Left: director $\mathbf{n}$ (as a line field) is shown on a vertical slice through Ω colored according to the degree of orientation s; the minimum value of s is 9.303×10^{-2}. The spherical inclusion is shown and the sub-domain Ω_1^* is depicted in black. Right: an oblique view of the same vertical slice with the $s = 0.2$ iso-surface shown.

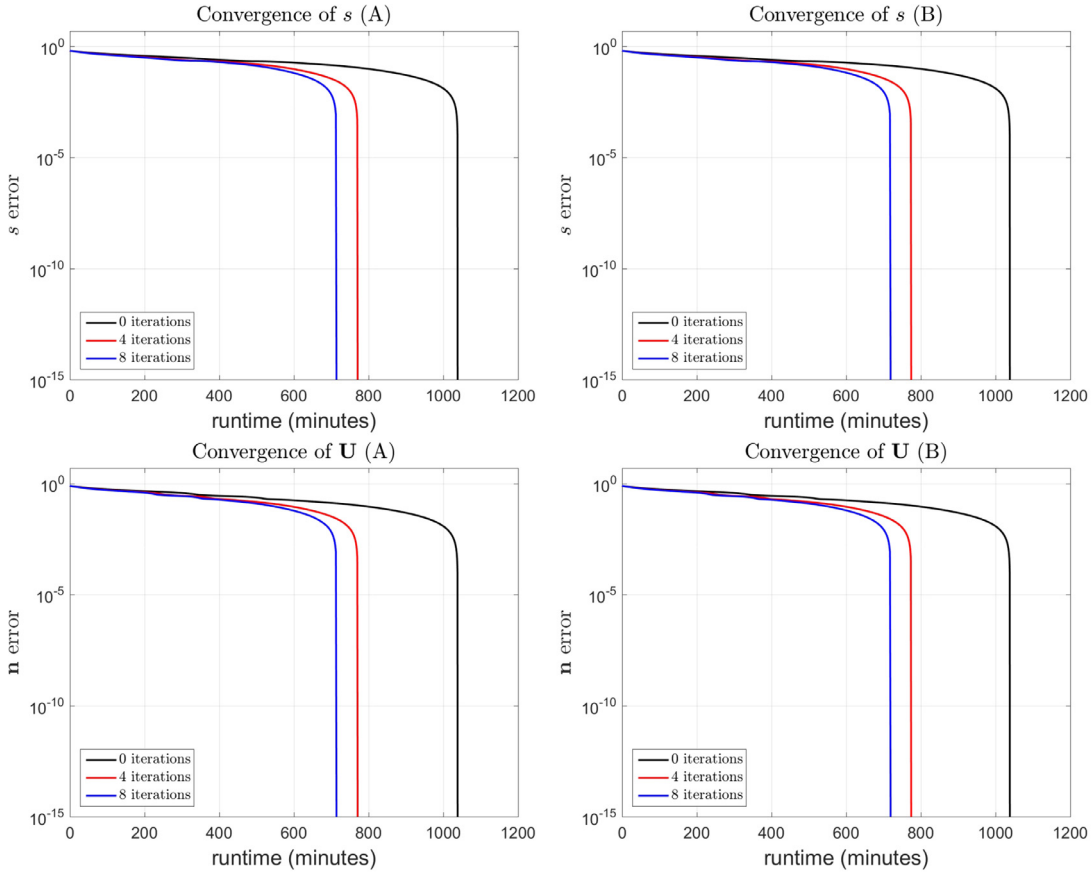

Fig. 9. Uniaxial LdG Saturn ring defect convergence results for s and $\mathbf{U}$ (Section 5.3.2) using the ℓ_∞ norm of the error. Plot (A) corresponds to $r_1 = 0.25$; Plot (B) corresponds to $r_1 = 0.5$. Number of iterations is for the singular sub-domain Ω_1^*.

The gradient flow schemes considered in this paper use an alternating direction approach, i.e. where we fix s and update $\mathbf{n}$ (or $\boldsymbol{\Theta}$) and vice-versa. This splitting of the variables leads to a kind of non-standard "stiffness" in the equations when defects are present. Our domain decomposition approach provides a way to augment the gradient flow scheme in a way to partially account for the non-linear/non-smooth stiffness caused by the degeneracy of defects. Note that when defects are not present, the gradient flow schemes converge to a minimizer in about 10 to 15 iterations without any domain decomposition technique.

The amount of acceleration varied between the two models, with the uniaxial LdG model benefiting a bit less. This is partially due to the fact that the uniaxially constrained LdG model is more complicated than the Ericksen model. This means the assembly of the discrete finite element matrices is more time-consuming in the uniaxial LdG model than in Ericksen. In order to obtain a reduction in computational run-time, one needs to take full advantage of having a smaller linear system to solve in the degenerate region, i.e. only assemble the necessary contributions to the matrix and reuse the known sparsity structure.

The performance of the DD approach presented here, with respect to changes in discretization parameters, has not been fully explored. The number of outer iterations (i.e. solving over the whole domain) is certainly reduced with the DD approach, but the total computational time

may not be improved. This is at least partly due to our implementation not being fully optimized. Again, assembly of the finite element matrices should be highly optimized to take advantage of this approach. Furthermore, since both models have non-convex energies, there can be some issue of convergence to a particular minimizer. But this is a typical issue in these models and is present regardless of what method is used to find the minimizer.

The DD technique can be combined with parallelization, such as when solving over the whole domain, i.e. a fixed decomposition of the entire domain can be used. Solving on the singular region could also be done in parallel, but there are issues of load balancing or of redistributing the degenerate region to the sub-processors. Other improvements of our technique could be to use more sub-domains, but more theoretical understanding of the method is needed to determine how best to partition the domain. Another option is to abandon the gradient flow scheme in the singular region, and use a global optimizer instead. If the singular region is not too large, then the added cost of a global optimizer could be mitigated.

Declaration of Competing Interest

The authors declare that they have no known competing financial interests or personal relationships that could have appeared to influence the work reported in this paper.

The authors declare the following financial interests/personal relationships which may be considered as potential competing interests:

References

[1] P.G. de Gennes, J. Prost, The Physics of Liquid Crystals, International Series of Monographs on Physics, 83, 2nd, Oxford Science Publication, Oxford, UK, 1995.

[2] J.P. Lagerwall, G. Scalia, A new era for liquid crystal research: applications of liquid crystals in soft matter nano-, bio- and microtechnology, Curr. Appl. Phys. 12 (6) (2012) 1387–1412, doi:10.1016/j.cap.2012.03.019.

[3] L. Blinov, Electro-Optical and Magneto-Optical Properties of Liquid Crystals, Wiley, 1983.

[4] J.W. Goodby, Handbook of Visual Display Technology (Editors: Chen, Janglin, Cranton, Wayne, Fihn, Mark), Springer, pp. 1290–1314.

[5] J. Sun, H. Wang, L. Wang, H. Cao, H. Xie, X. Luo, J. Xiao, H. Ding, Z. Yang, H. Yang, Preparation and thermo-optical characteristics of a smart polymer-stabilized liquid crystal thin film based on smectic A-chiral nematic phase transition, Smart Mater. Struct. 23 (12) (2014) 125038.

[6] J. Hoogboom, J.A. Elemans, A.E. Rowan, T.H. Rasing, R.J. Nolte, The development of self-assembled liquid crystal display alignment layers, Philos. Trans. R. Soc. Lond. A 365 (1855) (2007) 1553–1576, doi:10.1098/rsta.2007.2031.

[7] P. Dasgupta, M.K. Das, B. Das, Fast switching negative dielectric anisotropic multicomponent mixtures for vertically aligned liquid crystal displays, Mater. Res. Express 2 (4) (2015) 45015.

[8] J. Heo, J.-W. Huh, T.-H. Yoon, Fast-switching initially-transparent liquid crystal light shutter with crossed patterned electrodes, AIP Adv. 5 (4) (2015), doi:10.1063/1.4918277.

[9] M. Humar, I. Muševič, 3d microlasers from self-assembled cholesteric liquid-crystal microdroplets, Opt. Express 18 (26) (2010) 26995–27003, doi:10.1364/OE.18.026995.

[10] H. Coles, S. Morris, Liquid-crystal lasers, Nat. Photon. 4 (10) (2010) 676–685.

[11] F. Brochard, L. Léger, R.B. Meyer, Freedericksz transition of a homeotropic nematic liquid crystal in rotating magnetic fields, J. Phys. Colloques 36 (1975) C1–209–C1–213, doi:10.1051/jphyscol:1975139.

[12] , Flexoelectricity in Liquid Crystals: Theory, Experiments and Applications, Ágnes Buka, N. Éber (Eds.), World Scientific, 2012.

[13] A.A. Shah, H. Kang, K.L. Kohlstedt, K.H. Ahn, S.C. Glotzer, C.W. Monroe, M.J. Solomon, Self-assembly: liquid crystal order in colloidal suspensions of spheroidal particles by direct current electric field assembly (small 10/2012), Small 8 (10) (2012) 1551–1562, doi:10.1002/smll.201290056.

[14] J.K. Whitmer, X. Wang, F. Mondiot, D.S. Miller, N.L. Abbott, J.J. de Pablo, Nematic-field-driven positioning of particles in liquid crystal droplets, Phys. Rev. Lett. 111 (2013) 227801, doi:10.1103/PhysRevLett.111.227801.

[15] M. Wang, L. He, S. Zorba, Y. Yin, Magnetically actuated liquid crystals, Nano Letters 14 (7) (2014) 3966–3971, doi:10.1021/nl501302s. PMID: 24914876

[16] W. Zhu, M. Shelley, P. Palffy-Muhoray, Modeling and simulation of liquid-crystal elastomers, Phys. Rev. E 83 (2011) 051703, doi:10.1103/PhysRevE.83.051703.

[17] , Liquid Crystal Elastomers: Materials and Applications, in: W.H. de Jeu (Ed.), Advances in Polymer Science, Springer, 2012.

[18] J. Biggins, M. Warner, K. Bhattacharya, Elasticity of polydomain liquid crystal elastomers, J. Mech. Phys. Solids 60 (4) (2012) 573–590, doi:10.1016/j.jmps.2012.01.008.

[19] A. Rešetič, J. Milavec, B. Zupančič, V. Domenici, B. Zalar, Polymer-dispersed liquid crystal elastomers, Nat. Commun. 7 (2016) 13140, doi:10.1038/ncomms13140.

[20] M. Camacho-Lopez, H. Finkelmann, P. Palffy-Muhoray, M. Shelley, Fast liquid-crystal elastomer swims into the dark, Nat. Mater. 3 (5) (2004) 307–310.

[21] T.H. Ware, M.E. McConney, J.J. Wie, V.P. Tondiglia, T.J. White, Voxelated liquid crystal elastomers, Science 347 (6225) (2015) 982–984, doi:10.1126/science.1261019.

[22] C. Tschierske, Development of structural complexity by liquid-crystal self-assembly, Angew. Chem. Int. Ed. 52 (34) (2013) 8828–8878, doi:10.1002/anie.201300872.

[23] C. Blanc, Colloidal crystal ordering in a liquid crystal, Science 352 (6281) (2016) 40–41, doi:10.1126/science.aaf4260.

[24] I.I. Smalyukh, Liquid crystals enable chemoresponsive reconfigurable colloidal self-assembly, Proc. Natl. Acad. Sci. 107 (9) (2010) 3945–3946, doi:10.1073/pnas.1000312107.

[25] H.K. Bisoyi, S. Kumar, Liquid-crystal nanoscience: an emerging avenue of soft self-assembly, Chem. Soc. Rev. 40 (2011) 306–319, doi:10.1039/B901793N.

[26] J.A. Moreno-Razo, E.J. Sambriski, N.L. Abbott, J.P. Hernández-Ortiz, J.J. de Pablo, Liquid-crystal-mediated self-assembly at nanodroplet interfaces, Nature 485 (7396) (2012) 86–89, doi:10.1038/nature11084.

[27] M. Conradi, M. Ravnik, M. Bele, M. Zorko, S. Žumer, I. Muševič, Janus nematic colloids, Soft Matter 5 (2009) 3905–3912, doi:10.1039/B905631A.

[28] Z. Eskandari, N.M. Silvestre, M.M. Telo da Gama, Bonded boojum-colloids in nematic liquid crystals, Langmuir 29 (33) (2013) 10360–10367, doi:10.1021/la4017195. PMID: 23859624.

[29] R. James, J.-i. Fukuda, Effect of anchoring energy and elastic anisotropy on spherical inclusions in a nematic liquid crystal, Phys. Rev. E 88 (2013) 010501, doi:10.1103/PhysRevE.88.010501.

[30] S. Changizrezaei, C. Denniston, Heterogeneous colloidal particles immersed in a liquid crystal, Phys. Rev. E 95 (2017) 052703, doi:10.1103/PhysRevE.95.052703.

[31] I. Muševič, S. Žumer, Liquid crystals: maximizing memory, Nat. Mater. 10 (4) (2011) 266–268.

[32] T. Lopez-Leon, A. Fernandez-Nieves, Drops and shells of liquid crystal, Colloid Polym. Sci. 289 (4) (2011) 345–359, doi:10.1007/s00396-010-2367-7.

[33] S. Čopar, U. Tkalec, I. Muševič, S. Žumer, Knot theory realizations in nematic colloids, Proc. Natl. Acad. Sci. 112 (6) (2015) 1675–1680, doi:10.1073/pnas.1417178112.

[34] J.H. Adler, T.J. Atherton, T.R. Benson, D.B. Emerson, S.P. MacLachlan, Energy minimization for liquid crystal equilibrium with electric and flexoelectric effects, SIAM J. Sci. Comput. 37 (5) (2015) S157–S176, doi:10.1137/140975036.

[35] J.H. Adler, T.J. Atherton, D.B. Emerson, S.P. MacLachlan, An energy-minimization finite-element approach for the Frank–Oseen model of nematic liquid crystals, SIAM J. Numer. Anal. 53 (5) (2015) 2226–2254, doi:10.1137/140956567.

[36] J.H. Adler, D.B. Emerson, S.P. MacLachlan, T.A. Manteuffel, Constrained optimization for liquid crystal equilibria, SIAM J. Sci. Comput. 38 (1) (2016) B50–B76, doi:10.1137/141001846.

[37] S. Badia, F.M. Guillén-González, J.V. Gutiérrez-Santacreu, An overview on numerical analyses of nematic liquid crystal flows, Arch. Comput. Methods Eng. 18 (3) (2011) 285–313, doi:10.1007/s11831-011-9061-x.

[38] T. Davis, E. Gartland, Finite element analysis of the Landau-de Gennes minimization problem for liquid crystals, SIAM J. Numer. Anal. 35 (1) (1998) 336–362, doi:10.1137/S0036142996297448.

[39] M. Ravnik, S. Žumer, Landau-Degennes modelling of nematic liquid crystal colloids, Liq. Cryst. 36 (10–11) (2009) 1201–1214, doi:10.1080/02678290903056095.

[40] A. DeBenedictis, T.J. Atherton, Shape minimisation problems in liquid crystals, Liq. Cryst. 43 (13–15) (2016) 2352–2362, doi:10.1080/02678292.2016.1209699.

[41] A. Morvant, E. Seal, S.W. Walker, A coupled Ericksen/Allen-Cahn model for liquid crystal droplets, Comput. Math. Appl. 75 (11) (2018) 4048–4065, doi:10.1016/j.camwa.2018.03.013.

[42] A.E. Diegel, S.W. Walker, A finite element method for a phase field model of nematic liquid crystal droplets, Commun. Comput. Phys. 25 (2019) 155–188, doi:10.4208/cicp.OA-2017-0166.

[43] E.C. Gartland Jr, P. Palffy-Muhoray, R.S. Varga, Numerical minimization of the Landau-de Gennes free energy: defects in cylindrical capillaries, Mol. Cryst. Liq. Cryst. 199 (1) (1991) 429–452.

[44] S. Bartels, A. Raisch, Simulation of q-tensor fields with constant orientational order parameter in the theory of uniaxial nematic liquid crystals, in: M. Griebel (Ed.), Singular Phenomena and Scaling in Mathematical Models, Springer International Publishing, 2014, pp. 383–412, doi:10.1007/978-3-319-00786-1_17.

[45] I. Bajc, F. Hecht, S. Žumer, A mesh adaptivity scheme on the Landau-de Gennes functional minimization case in 3d, and its driving efficiency, J. Comput. Phys. 321 (2016) 981–996, doi:10.1016/j.jcp.2016.02.072.

[46] P.A. Cruz, M.F. Tomé, I.W. Stewart, S. McKee, Numerical solution of the Ericksen-Leslie dynamic equations for two-dimensional nematic liquid crystal flows, J. Comput. Phys. 247 (2013) 109–136, doi:10.1016/j.jcp.2013.03.061.

[47] F.M.G. González, J.V. Gutiérrez-Santacreu, A linear mixed finite element scheme for a nematic Ericksen-Leslie liquid crystal model, ESAIM 47 (2013) 1433–1464, doi:10.1051/m2an/2013076.

[48] R. James, E. Willman, F. FernandezFernandez, S.E. Day, Finite-element modeling of liquid-crystal hydrodynamics with a variable degree of order, IEEE Trans. Electron Dev. 53 (7) (2006) 1575–1582.

[49] X. Yang, M.G. Forest, H. Li, C. Liu, J. Shen, Q. Wang, F. Chen, Modeling and simulations of drop pinch-off from liquid crystal filaments and the leaky liquid crystal faucet immersed in viscous fluids, J. Comput. Phys. 236 (2013) 1–14, doi:10.1016/j.jcp.2012.10.042.

[50] X. Yang, M.G. Forest, C. Liu, J. Shen, Shear cell rupture of nematic liquid crystal droplets in viscous fluids, J. Non-Newtonian Fluid Mech. 166 (9–10) (2011) 487–499, doi:10.1016/j.jnnfm.2011.02.004.

[51] F. Alouges, A new algorithm for computing liquid crystal stable configurations: the harmonic mapping case, SIAM J. Numer. Anal. 34 (5) (1997) pp.1708–1726.
[52] J.W. Barrett, X. Feng, A. Prohl, Convergence of a fully discrete finite element method for a degenerate parabolic system modelling nematic liquid crystals with variable degree of orientation, ESAIM 40 (2006) 175–199, doi:10.1051/m2an:2006005.
[53] A. Ramage, E.C. GartlandJr., A preconditioned nullspace method for liquid crystal director modeling, SIAM J. Sci. Comput. 35 (1) (2013) B226–B247, doi:10.1137/120870219.
[54] N.J. Walkington, Numerical approximation of nematic liquid crystal flows governed by the Ericksen-Leslie equations, ESAIM 45 (2011) 523–540, doi:10.1051/m2an/2010065.
[55] R.H. Nochetto, S.W. Walker, W. Zhang, A finite element method for nematic liquid crystals with variable degree of orientation, SIAM J. Numer. Anal. 55 (3) (2017) 1357–1386, doi:10.1137/15M103844X.
[56] R.H. Nochetto, S.W. Walker, W. Zhang, Numerics for liquid crystals with variable degree of orientation, in: Symposium NN - Mathematical and Computational Aspects of Materials Science, in: MRS Proceedings, 1753, 2015, doi:10.1557/opl.2015.159.
[57] R.H. Nochetto, S.W. Walker, W. Zhang, The Ericksen model of liquid crystals with colloidal and electric effects, J. Comput. Phys. 352 (2018) 568–601, doi:10.1016/j.jcp.2017.09.035.
[58] WalkerShawn W., A finite element method for the generalized Ericksen model of nematic liquid crystals, ESAIM: M2AN 54 (4) (2020) 1181–1220, doi:10.1051/m2an/2019092.
[59] J. Zhao, Q. Wang, Semi-discrete energy-stable schemes for a tensor-based hydrodynamic model of nematic liquid crystal flows, J. Sci. Comput. 68 (3) (2016) 1241–1266, doi:10.1007/s10915-016-0177-x.
[60] J. Zhao, X. Yang, J. Shen, Q. Wang, A decoupled energy stable scheme for a hydrodynamic phase-field model of mixtures of nematic liquid crystals and viscous fluids, J. Comput. Phys. 305 (2016) 539–556, doi:10.1016/j.jcp.2015.09.044.
[61] J. Ericksen, Liquid crystals with variable degree of orientation, Arch. Rat. Mech. Anal. 113 (2) (1991) 97–120, doi:10.1007/BF00380413.
[62] J.M. Ball, E. Feireisl, F. Otto, Mathematical Thermodynamics of Complex Fluids, Lecture Notes in Mathematics book series (vol. 2200), Springer, 2015.
[63] J.-P. Borthagaray, R.H. Nochetto, S.W. Walker, A structure-preserving FEM for the uniaxially constrained **Q**-tensor model of nematic liquid crystals, in review (2019).
[64] J.-P. Borthagaray, S.W. Walker, The **Q**-tensor Model with Uniaxial Constraint, submitted (2019).
[65] L. Ambrosio, Existence of minimal energy configurations of nematic Liq. Cryst. with variable degree of orientation, Manuscr. Math. 68 (1) (1990) 215–228, doi:10.1007/BF02568761.
[66] F.H. Lin, On nematic liquid crystals with variable degree of orientation, Commun. Pure Appl. Math. 44 (4) (1991) 453–468, doi:10.1002/cpa.3160440404.
[67] A.M. Sonnet, E. Virga, Dissipative Ordered Fluids: Theories for Liquid Crystals, Springer, 2012.
[68] E.G. Virga, Variational Theories for Liquid Crystals, 8, 1st, Chapman and Hall, London, 1994.
[69] H. Mori, J. Eugene C. Gartland, J.R. Kelly, P.J. Bos, Multidimensional director modeling using the q tensor representation in a liquid crystal cell and its application to the pi-cell with patterned electrodes, Jpn. J. Appl. Phys. 38 (1R) (1999) 135.
[70] M. Paicu, A. Zarnescu, Energy dissipation and regularity for a coupled Navier-Stokes and q-tensor system, Arch. Rat. Mech. Anal. 203 (1) (2012) 45–67, doi:10.1007/s00205-011-0443-x.
[71] J.M. Ball, A. Zarnescu, Orientability and energy minimization in liquid crystal models, Arch. Rat. Mech. Anal. 202 (2) (2011) 493–535, doi:10.1007/s00205-011-0421-3.
[72] J.M. Ball, A. Zarnescu, Orientable and non-orientable director fields for liquid crystals, Proc. Appl. Math. Mech. 7 (1) (2007) 1050701–1050704, doi:10.1002/pamm.200700489.
[73] A. Majumdar, Equilibrium order parameters of nematic liquid crystals in the Landau-de Gennes theory, Eur. J. Appl. Math. 21 (2) (2010) 181–203, doi:10.1017/S0956792509990210.
[74] J.M. Ball, Mathematics and liquid crystals, Mol. Cryst. Liq. Cryst. 647 (1) (2017) 1–27, doi:10.1080/15421406.2017.1289425.
[75] F.C. Frank, I. Liquid crystals. On the theory of liquid crystals, Discuss. Faraday Soc. 25 (1958) 19–28, doi:10.1039/DF9582500019.
[76] D. Kinderlehrer, N. Walkington, B. Ou, The Elementary Defects of the Oseen-Frank Energy for a Liquid Crystal, Research report (Carnegie Mellon University. Department of Mathematics. Center for Nonlinear Analysis), Carnegie Mellon University, Department of Mathematics [Center for Nonlinear Analysis], 1993.
[77] R. Perkins, Liquid Crystal, 2009. (http://www.teachersource.com/downloads/lesson_pdf/LC-AST.pdf)
[78] B. Senyuk, Liquid Crystals: A Simple View on a Complex Matter, 2010. (http://www.personal.kent.edu/bisenyuk/liquidcrystals/).
[79] E.B. Priestley, P.J. Wojtowicz, P. Sheng, Introduction to Liquid Crystals, Plenum Press New York, 1975.
[80] J. Eugene C. Gartland, Scalings and limits of Landau-de Gennes models for liquid crystals: a comment on some recent analytical papers, Math. Modell. Anal. 23 (3) (2018) 414–432, doi:10.3846/mma.2018.025.
[81] M. Calderer, D. Golovaty, F. Lin, C. Liu, Time evolution of nematic liquid crystals with variable degree of orientation, SIAM J. Math. Anal. 33 (5) (2002) 1033–1047, doi:10.1137/S0036141099362086.
[82] N.J. Mottram, C.J.P. Newton, Introduction to Q-tensor theory, ArXiv e-prints (2014).
[83] B.R. Acharya, A. Primak, S. Kumar, Biaxial nematic phase in bent-core thermotropic mesogens, Phys. Rev. Lett. 92 (2004) 145506, doi:10.1103/PhysRevLett.92.145506.
[84] L.A. Madsen, T.J. Dingemans, M. Nakata, E.T. Samulski, Thermotropic biaxial nematic liquid crystals, Phys. Rev. Lett. 92 (2004) 145505, doi:10.1103/PhysRevLett.92.145505.
[85] V. Prasad, S.-W. Kang, K. Suresh, L. Joshi, Q. Wang, S. Kumar, Thermotropic uniaxial and biaxial nematic and smectic phases in bent-core mesogens, J. Am. Chem. Soc. 127 (49) (2005) 17224–17227.
[86] P. Palffy-muhoray, E.C. Gartland, J.R. Kelly, A new configurational transition in inhomogeneous nematics, Liq. Cryst. 16 (4) (1994) 713–718, doi:10.1080/02678299408036543.
[87] A. Sonnet, A. Kilian, S. Hess, Alignment tensor versus director: description of defects in nematic liquid crystals, Phys. Rev. E 52 (1995) 718–722, doi:10.1103/PhysRevE.52.718.
[88] X. Lamy, A new light on the breaking of uniaxial symmetry in nematics, ArXiv e-prints (2013).
[89] S. Bartels, Numerical Methods for Nonlinear Partial Differential Equations, Springer Series in Computational Mathematics, first ed., Springer, 2015.
[90] S.M. Wise, C. Wang, J.S. Lowengrub, An energy-stable and convergent finite-difference scheme for the phase field crystal equation, SIAM J. Numer. Anal. 47 (3) (2009) 2269–2288, doi:10.1137/080738143.
[91] J. Xu, Y. Li, S. Wu, A. Bousquet, On the stability and accuracy of partially and fully implicit schemes for phase field modeling, Comput. Methods Appl. Mech. Eng. 345 (2019) 826–853, doi:10.1016/j.cma.2018.09.017.
[92] S.W. Walker, FELICITY: a Matlab/C++ toolbox for developing finite element methods and simulation modeling, SIAM J. Sci. Comput. 40 (2) (2018) C234–C257, doi:10.1137/17M1128745.
[93] Y. Notay, An aggregation-based algebraic multigrid method, Electron. Trans. Numer. Anal. 37 (2010) 123–146.
[94] A. Napov, Y. Notay, Algebraic analysis of aggregation-based multigrid, Numer. Linear Algebra Appl. 18 (3) (2011) 539–564, doi:10.1002/nla.741.
[95] A. Napov, Y. Notay, An algebraic multigrid method with guaranteed convergence rate, SIAM J. Sci. Comput. 34 (2) (2012) A1079–A1109, doi:10.1137/100818509.
[96] Y. Notay, Aggregation-based algebraic multigrid for convection-diffusion equations, SIAM J. Sci. Comput. 34 (4) (2012) A2288–A2316, doi:10.1137/110835347.
[97] Y. Gu, N.L. Abbott, Observation of saturn-ring defects around solid microspheres in nematic liquid crystals, Phys. Rev. Lett. 85 (2000) 4719–4722, doi:10.1103/PhysRevLett.85.4719.
[98] S. Alama, L. Bronsard, X. Lamy, Analytical description of the saturn-ring defect in nematic colloids, Phys. Rev. E 93 (2016) 012705, doi:10.1103/PhysRevE.93.012705.